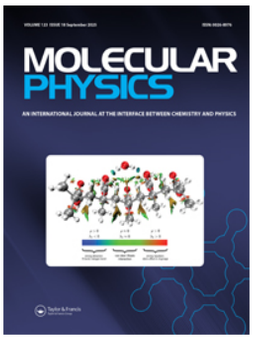

Taylor & Francis
Taylor & Francis Group

Molecular Physics

An International Journal at the Interface Between Chemistry and Physics

ISSN: 0026-8976 (Print) 1362-3028 (Online) Journal homepage: www.tandfonline.com/journals/tmph20

Extending the SAFT-γ Mie group-contribution approach to model cyclic ketones: application to monoterpenoids

Shubhani Paliwal, Felipe A. Perdomo, Thomas Bernet, Ahmed Alyazidi, Andrew J. Haslam, George Jackson & Amparo Galindo

To cite this article: Shubhani Paliwal, Felipe A. Perdomo, Thomas Bernet, Ahmed Alyazidi, Andrew J. Haslam, George Jackson & Amparo Galindo (11 May 2025): Extending the SAFT-γ Mie group-contribution approach to model cyclic ketones: application to monoterpenoids, Molecular Physics, DOI: 10.1080/00268976.2025.2493320

To link to this article: https://doi.org/10.1080/00268976.2025.2493320

© 2025 The Author(s). Published by Informa UK Limited, trading as Taylor & Francis Group.

Published online: 11 May 2025.

Submit your article to this journal

Article views: 665

View related articles

View Crossmark data

Full Terms & Conditions of access and use can be found at
https://www.tandfonline.com/action/journalInformation?journalCode=tmph20

MOLECULAR PHYSICS e2493320
https://doi.org/10.1080/00268976.2025.2493320

Taylor & Francis
Taylor & Francis Group

THERMODYNAMICS 2024 CONFERENCE (BY INVITATION ONLY)

OPEN ACCESS Check for updates

Extending the SAFT-γ Mie group-contribution approach to model cyclic ketones: application to monoterpenoids

Shubhani Paliwal, Felipe A. Perdomo, Thomas Bernet, Ahmed Alyazidi, Andrew J. Haslam, George Jackson and Amparo Galindo

Department of Chemical Engineering, Sargent Centre for Process Systems Engineering, Institute for Molecular Science and Engineering, Imperial College London, London, UK

ABSTRACT

Monoterpenoids such as menthone are essential in organic synthesis, pharmaceuticals, and the fragrance industry for their versatile roles in developing complex molecules, flavours, and therapeutic agents. We extend the capability of the SAFT-γ Mie group-contribution equation of state by developing a new cyclic-ketone group, denoted as cCO, featuring two electron lone-pair sites that can interact with electropositive hydrogen sites in other associating compounds. The model parameters of the new cCO group are refined to represent target experimental thermophysical data of pure cyclic ketones, including the vapour pressure, single-phase density, heat capacity, and vaporisation enthalpy, as well as mixture data including the excess enthalpy, liquid density, vapour–liquid, liquid–liquid, and solid–liquid equilibria. New parameters that characterise the group interactions (one like interaction and 16 unlike interactions) are developed and used to calculate these thermophysical properties. We evaluate the robustness of the newly developed group and its transferability to other compounds, focussing on pure cyclobutanone, cyclopentanone, cyclohexanone, cycloheptanone, and cyclooctanone, and their mixtures with hydrocarbons, alcohols, ketones, esters, aromatic compounds, and water. The theoretical calculations and found to be in good agreement with experiment, and the final model allows for accurate predictions of thermodynamic properties and complex phase behaviour, including azeotrope compositions. Morever, we transfer the parameters developed for the cyclic ketone group to predict the properties of pure 3-methylcyclohexanone and menthone, as well as the phase behaviour of binary mixtures of menthone with menthol and water, finding good agreement with available experimental data.

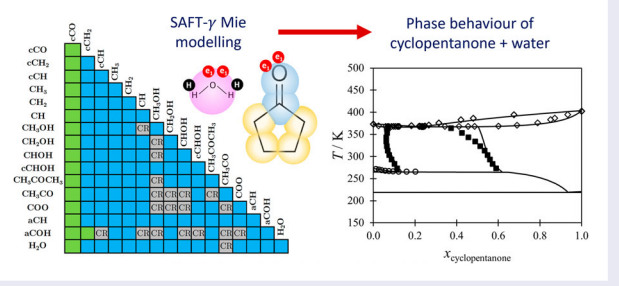

ARTICLE HISTORY
Received 8 January 2025
Accepted 10 April 2025

KEYWORDS
SAFT-γ Mie; equation of state; phase behaviour; cyclic ketones; monoterpenoids

1. Introduction

Thermodynamic modelling tools play a vital role in industrial process design and development by facilitating the prediction of thermodynamic properties at conditions that can span broad ranges of temperature, pressure, and composition, including multicomponent mixtures, and varied type of phase equilibria (vapour–liquid, liquid–liquid, and solid–liquid), thus reducing the need for experimental trials. Group-contribution methods, in which the physical, chemical, and thermodynamic properties of substances are predicted from knowledge of the characteristics of the functional groups present in the molecules are especially attractive as predictive tools as they simplify the modelling of complex systems. They are widely used in phase-behaviour prediction and property estimation in the chemical and pharmaceutical industries, although they can lack precision as they often rely on the assumption that group effects are additive.

CONTACT Amparo Galindo a.galindo@imperial.ac.uk Department of Chemical Engineering, Sargent Centre for Process Systems Engineering, Institute for Molecular Science and Engineering, Imperial College London, South Kensington Campus, London SW7 2AZ, UK

© 2025 The Author(s). Published by Informa UK Limited, trading as Taylor & Francis Group.
This is an Open Access article distributed under the terms of the Creative Commons Attribution License (http://creativecommons.org/licenses/by/4.0/), which permits unrestricted use, distribution, and reproduction in any medium, provided the original work is properly cited. The terms on which this article has been published allow the posting of the Accepted Manuscript in a repository by the author(s) or with their consent.

Moreover, their applicability and accuracy are limited by the availability of reliable group parameters.

One of the most successful group-contribution methods for the prediction of properties in fluid mixtures is the UNIFAC approach [1]. In this approach, molecules are divided into structural groups and their activity coefficients are calculated based on group interactions. UNIFAC has been shown to be very accurate for phase-equilibrium predictions such as vapour–liquid equilibria (VLE), when combined with an equation of state, and liquid–liquid equilibria (LLE). The UNIFAC model has also been used in the development of predictive group-contribution equations of state, such as the predictive SRK equation [2], which combine the predicted ability of UNIFAC to determine the unlike (k_{ij}) molecular parameters of the equation of state to predict phase equilibria in gases and liquids. More recently, COSMO-SAC [3], in which group-contribution concepts are combined with quantum chemistry to predict mixture phase equilibria, has emerged.

While UNIFAC, PSRK, and COSMO-SAC are powerful thermodynamic predictive methods, they find limited agreement in some systems. UNIFAC can lead to large deviations in the case of highly polar and hydrogen-bonding systems, and mixtures comprising molecules of very disparate size. Importantly, as it is an activity-coefficient method, it relies on coupling with an equation of state to model vapour–liquid equilibra. The PSRK, as an equation of state, does not have this limitation, but also leads to a loss of accuracy when modelling mixtures involving polar and hydrogen-bonding molecules due to the limitations of the underlying cubic equation of state on which it relies. COSMO-SAC requires computationally intensive quantum-chemistry calculations for new compounds and can be limited by the accuracy of the underlying quantum-chemical methods for large or flexible molecules.

In this context, the SAFT-γ Mie group-contribution equation of state [4–7] offers greater accuracy by considering molecular size, shape, and incorporating hydrogen-bonding interactions. The statistical associating fluid theory (SAFT) [8, 9] was developed in the late 1980s, and since then a number of versions have been formulated. Among these is the SAFT-VR [10] approach, of which SAFT-γ Mie is the latest descendant. It is the group-contribution reformulation of the SAFT-VR Mie [11] equation of state, in which the interactions between the segments forming the model molecules are described using Mie (generalised Lennard-Jones) potentials, and a third-order high-temperature expansion of the attractive contributions to the free energy is incorporated. In the SAFT-γ Mie approach compounds are represented as chains of fused segments that are not necessarily identical; i.e. a heteronuclear chain model is implemented. The segments feature association sites when appropriate to incorporate directional interactions that mimic hydrogen bonds. It can be used predictively to describe a broad variety of thermodynamic properties, including second-order derivative properties [12–14], and it can be used for the prediction of vapour–liquid, liquid–liquid and solid–liquid phase behaviour of complex systems with high accuracy [14]. In pharmaceutical applications, Febra et al. [15] developed group interactions for mefenamic acid, diphenylamine, and benzoic acid, and assessed the transferability of the group interactions by comparison with experimental solubility data. Wehbe et al. [16] extended the approach to study the pH-solubility of aqueous solutions of ibuprofen and ketoprofen. The thermodynamic properties of other complex mixtures such as lactone [17], polymers [18, 19], amino acids and peptides [20], and compounds relevant for carbon capture [21, 22] have also been considered in previous work with this approach. An added advantage of the group-contribution nature of SAFT-γ Mie is its application in computer-aided process design, in relation to pharmaceutical processes [23], organic Rankine cycles [24], and CO_2 capture [25–30].

In the current work we consider terpenes, a class of organic compounds that are of interest for their wide range of biological activity in pharmaceuticals, and in applications in fragrances and flavours. Monoterpenoids [31] in particular are modified terpenes consisting of two isoprene units typically with a ten-carbon backbone that includes chemical functionality such as alcohols, carboxylic acids, or ketones, giving them unique chemical properties. They exhibit hydrophobicity making them insoluble in water, while also having varying degrees of polarity that make them soluble in organic solvents such as ethanol and ethyl acetate [32]. Modelling these compounds is challenging due to their structural complexity (cyclic, branched, and unsaturated), and highly polarisable nature, which leads to highly non-ideal intermolecular interactions in solvents.

As an example, menthone ((2S,5R)-trans-2-isopropyl-5-methyl cyclohexanone) contains a carbonyl group, an isopropyl group, and a methyl group, as shown in Figure 1. Four unique stereoisomers are possible for the structure of menthone: (−)-menthone, (+)-menthone, (+)-isomenthone, and (−)-isomenthone. Of these, *l*-menthone ((−)-menthone) is the most abundant in nature, which we refer to simply as menthone in the current work. It has a characteristic minty odour that has led to its widespread industrial use in fragrances [33–37], flavourings [38–41], and cosmetics [42]. It has also been shown to have anti-bacterial and anti-fungal effects [43, 44]. Its potential for use in the medical industry has been

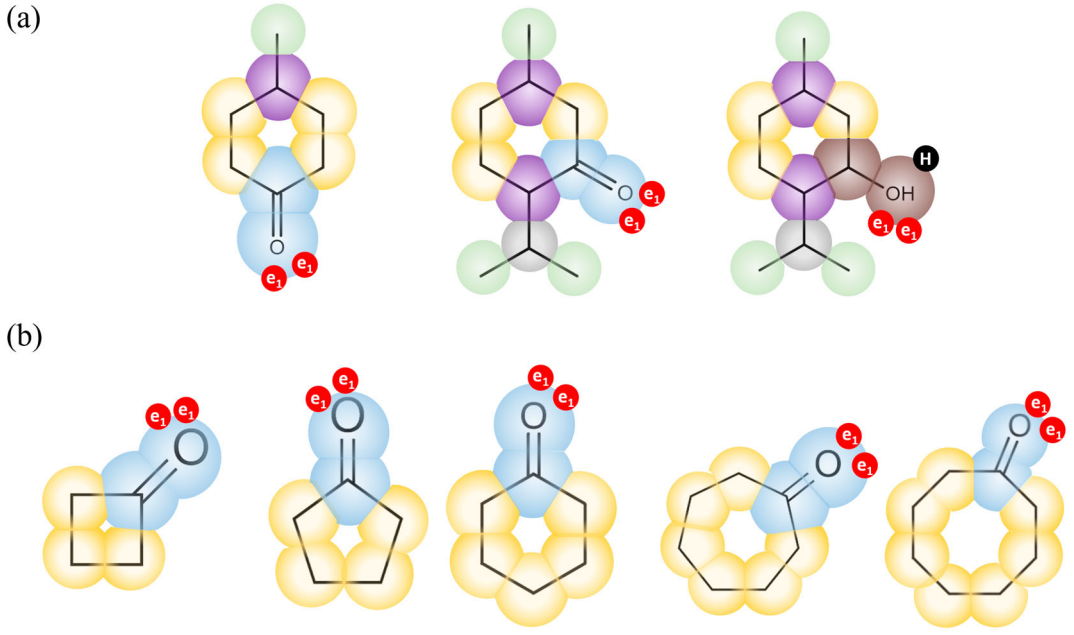

Figure 1. Molecular representation and SAFT-γ Mie molecular model of (a) 3-methylcyclohexanone (left), menthone (centre), and menthol (right), and (b) cyclic ketones: cyclobutanone (left) to cyclooctanone (right). The new cCO group (blue) is decorated with two association sites denoted by the smaller red circles, labelled e_1 for electronegative (acceptor) sites. The cCHOH group (brown) is decorated with two e_1 sites and one site of type H. cCH_2 groups are coloured yellow, cCH groups purple, CH groups grey, and CH_3 groups green.

recognised through studies indicating its efficacy as an anti-inflammatory [45, 46] and as an anti-depressant [47, 48] ; it has also been found to be useful in the medical treatment by dissolution of gall-bladder stones [49].

The phase behaviour of menthone and its mixtures has been previously studied using the NRTL [50], UNIQUAC [51], Wilson [52], and COSMO-RS [53] approaches [54, 55]. In the work of Batiu [54], the VLE of binary mixtures involving *n*-decane and menthone were measured and analysis of the VLE data was carried out by implementing the Wilson, UNIQUAC, and NRTL models. The binary parameters for the models were estimated from the experimental VLE data, with the calculations shown to be in good agreement with the measured data. In the work of Vilas-Boas et al. [55], the octanol–water partition coefficient and aqueous solubility of menthone were measured using the traditional shake-flask method. Solubility predictions have also been presented using the COSMO-RS method, the Abraham solvation model [56, 57], and the ACD/Log P tool [58].

In recent work, we extended the applicability of SAFT-γ Mie to model another monoterpenoid, i.e. menthol, and provided reliable predictions of the thermophysical properties of menthol in a range of solvents. Here, we use the SAFT-γ Mie approach to model cyclic ketones and menthone, and calculate the thermodynamic properties and phase behaviour of these pure compounds and their binary mixtures in a range of solvents. A new cyclic-ketone cCO group is developed to model both menthone and simple cyclic ketones. A description of the SAFT-γ Mie approach, model development for the systems of interest, and parameter estimation are detailed in Section 2. Thermodynamic-property calculations for pure cyclic ketones and mixtures of cyclic ketones in several solvents are presented in Section 3. Predictive calculations of properties such as the vapour pressure for pure menthone and 3-methyl cyclohexanone, and the VLE of mixtures including menthone are presented in Section 4. The performance of the model is presented and discussed in Section 5. Conclusions and additional comments are given in Section 6.

2. Methodology

2.1. SAFT-γ Mie model and theory

SAFT-γ Mie [4–7] is a group-contribution approach based on a hetero-nuclear model of fused segments interacting via Mie potentials given as [59]

$$\Phi_{kl}^{\mathrm{Mie}}(r_{kl}) = \mathcal{C}_{kl}\varepsilon_{kl}\left[\left(\frac{\sigma_{kl}}{r_{kl}}\right)^{\lambda_{kl}^{\mathrm{r}}} - \left(\frac{\sigma_{kl}}{r_{kl}}\right)^{\lambda_{kl}^{\mathrm{a}}}\right], \qquad (1)$$

where r_{kl} is the centre–centre separation of segments k and l, σ_{kl} is a size parameter (which corresponds to the segment diameter in the case of like interactions ($k = l$)), ε_{kl} is the depth of the potential well, and $\lambda_{kl}^{\mathrm{r}}$ and $\lambda_{kl}^{\mathrm{a}}$

are the repulsive and attractive exponents of the interaction between the segments, respectively. The prefactor C_{kl}, given by

$$C_{kl} = \frac{\lambda_{kl}^{\mathrm{r}}}{\lambda_{kl}^{\mathrm{r}} - \lambda_{kl}^{\mathrm{a}}} \left(\frac{\lambda_{kl}^{\mathrm{r}}}{\lambda_{kl}^{\mathrm{a}}}\right)^{\frac{\lambda_{kl}^{\mathrm{a}}}{\lambda_{kl}^{\mathrm{r}} - \lambda_{kl}^{\mathrm{a}}}}, \tag{2}$$

ensures that the minimum of the interaction is $-\varepsilon_{kl}$.

The SAFT-γ Mie representations of 3-methylcyclohexanone, menthone, and menthol, along with the cyclic ketones considered in our work are presented in Figure 1. A compound i is represented by its different chemical moieties k, each corresponding to a group k. The number of occurrences of a group of type k is accounted by ν_k. The number of segments fused in a functional group is denoted by ν_k^*. A functional group is fully characterised by its Mie potential parameters ε_{kk}, σ_{kk}, $\lambda_{kk}^{\mathrm{r}}$ and $\lambda_{kk}^{\mathrm{a}}$, and the shape factor S_k (which characterises the extent of the contribution of a group k to the properties of the compound). Segments can also feature short-ranged square-well association sites when necessary to incorporate directional interactions that mimic hydrogen bonds. For these site–site association interactions, the association energy $\varepsilon_{kk,ab}^{\mathrm{HB}}$, the bonding volume $K_{kk,ab}^{\mathrm{HB}}$, the number of different site types $N_{\mathrm{ST},k}$, and the number of sites of each type $n_{k,a}, n_{k,b},\ldots, n_{k,N_{\mathrm{ST},k}}$ are also required. The unlike interactions between group k and group l are described through the parameters σ_{kl}, ε_{kl}, $\lambda_{kl}^{\mathrm{r}}$, and $\lambda_{kl}^{\mathrm{a}}$; $\varepsilon_{kl,ab}^{\mathrm{HB}}$ and $K_{kl,ab}^{\mathrm{HB}}$ are also required if a site-site association interaction is present.

The dimensionless form of the total Helmholtz free energy A of a mixture consisting of non-ionic compounds is given as

$$\frac{A}{Nk_{\mathrm{B}}T} = \frac{A^{\mathrm{ideal}}}{Nk_{\mathrm{B}}T} + \frac{A^{\mathrm{mono.}}}{Nk_{\mathrm{B}}T} + \frac{A^{\mathrm{chain}}}{Nk_{\mathrm{B}}T} + \frac{A^{\mathrm{assoc.}}}{Nk_{\mathrm{B}}T}, \tag{3}$$

where A^{ideal} represents the ideal-free-energy contribution, $A^{\mathrm{mono.}}$ represents contribution corresponding to the interactions between the monomer Mie segments, A^{chain} represents the contribution of chain formation of monomer Mie segments, and $A^{\mathrm{assoc.}}$ represents contribution from association interactions. N is the total number of molecules, T the temperature of the system, and k_{B} the Boltzmann constant. The expressions used to calculate each term are detailed in previous work [4–7].

Once the functional form of the Helmholtz free energy is fully specified, other properties can be easily determined using standard thermodynamic relations [60]. In particular, the pressure $P = -(\partial A/\partial V)_{T,N}$, where V is the system volume, and chemical potential $\mu_i = (\partial A/\partial N_i)_{T,V,N_{j\neq i}}$ of each species i, with the total Gibbs free energy $G = A + PV = \sum_{i=1}^{N_{\mathrm{C}}} N_i\mu_i$ (where N_{C} is the number of components), are used to determine the phase equilibria of the systems of interest by implementing the Helmholtz free-energy Lagrangian dual (HELD) algorithm [61, 62], an isothermal P,T flash algorithm for the identification of all the stable phases and the composition of mixtures coexisting at equilibrium. The solubility (solid–liquid equilibrium (SLE)) of a compound i is defined by its molar fraction x^{sat} in the saturated solution, in coexistence with a solid phase assumed to be pure i. It can be calculated from [15]

$$\begin{aligned}\ln x_i^{\mathrm{sat}}(T,P,\mathbf{x}^{\mathrm{sat}}) = &-\frac{\Delta h_i^{\mathrm{fus}}(T_i^{\mathrm{fus}},P)}{R}\left(\frac{1}{T}-\frac{1}{T_i^{\mathrm{fus}}}\right)\\ &-\frac{\Delta c_{p,i}(T_i^{\mathrm{fus}},P)}{R}\\ &\times\left(\ln\frac{T_i^{\mathrm{fus}}}{T}-\frac{T_i^{\mathrm{fus}}}{T}+1\right)\\ &-\ln\gamma_i(T,P,\mathbf{x}^{\mathrm{sat}}).\end{aligned} \tag{4}$$

The melting temperature T_i^{fus} and the enthalpy of fusion $\Delta h_i^{\mathrm{fus}}$ of the compounds for which solid–liquid solubility is calculated here are given in Table 1. Experimental data for the difference in the heat capacity of the liquid and solid phase at the melting temperature $\Delta c_{p,i}(T_i^{\mathrm{fus}},P)$ of pure compounds is often not available in the literature and thus $\Delta c_{p,i}(T_i^{\mathrm{fus}},P)$ is neglected in the calculations performed in our current work.

Table 1. Molar enthalpy of fusion $\Delta h_i^{\mathrm{fus}}$ and melting temperature T_i^{fus} of cyclic ketones, water, menthone, and menthol, used in the SAFT-γ Mie solubility predictions in the current work.

Compound i	$\Delta h_i^{\mathrm{fus}}$ / (kJ/mol)	T_i^{fus} / K	Ref.
cyclopentanone	1.14	221	[63]
cyclohexanone	1.19	242	[64]
cycloheptanone	1.39	252	[64, 65]
water	6.02	273.15	[66]
menthone	18.5	267.15	[67, 68]
menthol	12.3	316	[69]

2.2. Parameter optimisation

To estimate the like and unlike group–group interactions, experimental data for pure compounds and mixtures are considered. For pure compounds, the vapour pressure, saturated-vapour and liquid densities, isobaric densities, heat capacities, and enthalpy of vaporisation are considered. For mixtures, VLE, LLE, liquid density, and liquid excess enthalpy data are considered to refine the interaction parameters. SLE data are not included in parameter estimation and are only used to assess the predictive capability of the models developed. An objective function f_{obj} is minimised to obtain the parameters characterising the

interactions between two groups k and l; i.e.

$$\min_{\Theta} f_{\text{obj}} = \sum_{s=1}^{N^{\text{S}}} \sum_{p=1}^{N_s^{\text{P}}} \sum_{i=1}^{N_{s,p}^{\text{D}}} w_{s,p,i} \times \left(\left(\frac{X_{s,p,i}^{\text{exp.}} - X_{s,p,i}^{\text{calc.}}(\Theta)}{X_{s,p,i}^{\text{exp.}}} \right) \times 100 \right)^2, \quad (5)$$

where Θ represents the vector of estimated parameters. The number of systems used in the estimation is represented by N^{S}, the number of types of property for system s is represented by N_s^{P}, and the number of experimental data points for system s and property p is represented by $N_{s,p}^{\text{D}}$. An equal weight is given to each experimental data point ($w_{s,p,i} = 1$). The i^{th} measured value of property p of system s, and the corresponding calculated value with SAFT-γ Mie are represented by $X_{s,p,i}^{\text{exp.}}$ and $X_{s,p,i}^{\text{calc.}}(\Theta)$, respectively. This optimisation problem is solved using gPROMS Properties 2.6.0 [70].

The accuracy of the description of a calculated property $X^{\text{calc.}}$ consisting of n^{X} data points when compared to the experimental data $X^{\text{exp.}}$ is verified by calculating AAD and %AAD, defined respectively as

$$\text{AAD } X = \frac{1}{n^{\text{X}}} \sum_{i=1}^{n^{\text{D}}} \left| X_i^{\text{exp.}} - X_i^{\text{calc.}} \right|, \quad (6)$$

and

$$\%\text{AAD } X = \frac{1}{n^{\text{X}}} \sum_{i=1}^{n^{\text{D}}} \left| \frac{X_i^{\text{exp.}} - X_i^{\text{calc.}}}{X_i^{\text{exp.}}} \right| \times 100. \quad (7)$$

3. Cyclic ketones and solvent modelling

In the following subsections, we present selected examples of thermodynamic-property calculations carried out using the SAFT-γ Mie equation of state for pure cyclic ketones and their mixtures with a range of solvents for which experimental data [71–134] are available. We provide parameter-estimation and calculation details for pure cyclic ketones and binary mixtures of cyclic ketones with cyclic alkanes, primary alcohols, cyclic alcohols, water, and branched cyclic ketones. We have also carried out calculations of the thermodynamic properties of binary mixtures of cyclic ketones with linear and branched alkanes, secondary and branched alcohols, acetone, secondary ketones, esters, and aromatic compounds. In the interest of brevity, details of the latter calculations are omitted, with only the quantitative measures of the corresponding deviations, in terms of the AAD and ADD%, summarised in Table 7.

3.1. Pure cyclic ketones and cyclic ketone + cyclic alkane mixtures: cCO–cCO and cCO–cCH$_2$ interactions

The cyclic ketones considered here are four- to eight-membered rings consisting of a ketone functional group within the cyclic structure. The SAFT-γ Mie models for cyclobutanone to cyclooctanone are described in Table 2. The cyclic ketones are modelled with one cyclic ketone group cCO, and three to seven cyclic alkane groups cCH$_2$ for cyclobutanone to cyclooctanone, respectively. We develop a new cyclic ketone group, cCO, to model this family of compounds. The cCO group includes two electronegative sites, labelled as e$_1$, corresponding to the oxygen lone electron pairs; these e$_1$ sites are allowed to bond with H sites of associating functional groups, if present in the solvents. In similar fashion, linear 2-ketones are represented with the CH$_3$CO group [15] and also include two association sites of type e$_1$. The cCH$_2$ group that has been developed in previous work [5] is transferred here to model this family of compounds. The SAFT-γ Mie models for cyclic alkanes comprise cCH$_2$ functional groups only.

The group interaction submatrix pertinent to our current work is presented in Table 3; this includes interactions developed in previous work [4–7, 13–15, 17, 21, 135–137] and interactions (not relevant to our current work) that are calculated using combining rules [4]. The new parameter values characterising the cCO group and all the other functional groups present in the solvents that are considered in our current work are presented in Tables 4–6.

Experimental data for the vapour pressure [138–142], saturated-liquid density [143–146], isobaric-liquid density [141], isobaric heat capacity, [63, 147, 148], and enthalpy of vaporisation [144, 149] are available for cyclic ketones. Liquid excess-enthalpy data for cyclohexanone + cyclopentane [71, 78] and cyclohexanone + cyclohexane [150] at $T = 298.15$ K and $P = 101.3$ kPa, isobaric VLE data for cyclohexanone + cyclohexane [151] at $P = 101.3$ kPa, isothermal VLE data for cyclohexanone + cyclohexane [152] at $T = 348.15$ K, and liquid-density data for cyclohexanone + cyclohexane [153] at $T = 298.15$ K, 303.15 K, and 308.15 K are also available. We consider the vapour pressure [139, 140, 142] and saturated-liquid density [143, 145] of cyclopentanone and cyclohexanone, along with the excess enthalpy and liquid-density data [150] of cyclohexanone + cyclohexane to estimate the interaction parameters. The remaining experimental data are used to test the transferability of the optimised parameters in predictions of the thermodynamic properties of other systems.

Table 2. List of compounds considered in our current work, together with the SAFT-γ Mie group representation.

Compound	CAS number	Molecular formula	SAFT-γ Mie model
menthone	14073-97-3	$C_{10}H_{18}O$	cCH_2 (×3), cCO, cCH (×2), CH, CH_3 (×3)
menthol	1490-04-6	$C_{10}H_{20}O$	cCH_2 (×3), cCHOH, cCH (×2), CH, CH_3 (×3)
cyclic ketones (cyclobutanone ($n = 4$) to cyclooctanone ($n = 8$))	N/A	$C_nH_{2n-2}O$	cCH_2 (×($n - 1$)), cCO, for $n \geq 4$
3-methylcyclohexanone	591-24-2	$C_7H_{12}O$	cCH_2 (×4), cCH, cCO, CH_3
cyclopentane	287-92-3	C_5H_{10}	cCH_2 (×5)
cyclohexane	110-82-7	C_6H_{12}	cCH_2 (×6)
cycloheptane	291-64-5	C_7H_{14}	cCH_2 (×7)
1-alcohols (ethanol ($n = 2$), propan-1-ol ($n = 3$), etc.)	N/A	$C_nH_{2n+2}O$	CH_3, CH_2 (×($n - 2$)), CH_2OH, for $n \geq 2$
cyclopentanol	96-41-3	$C_5H_{10}O$	cCH_2 (×4), cCHOH
cyclohexanol	108-93-0	$C_6H_{12}O$	cCH_2 (×5), cCHOH
water	7732-18-5	H_2O	H_2O

Table 3. Summary of the group interactions used to model cyclic ketones in a range of solvents with the SAFT-γ Mie approach.

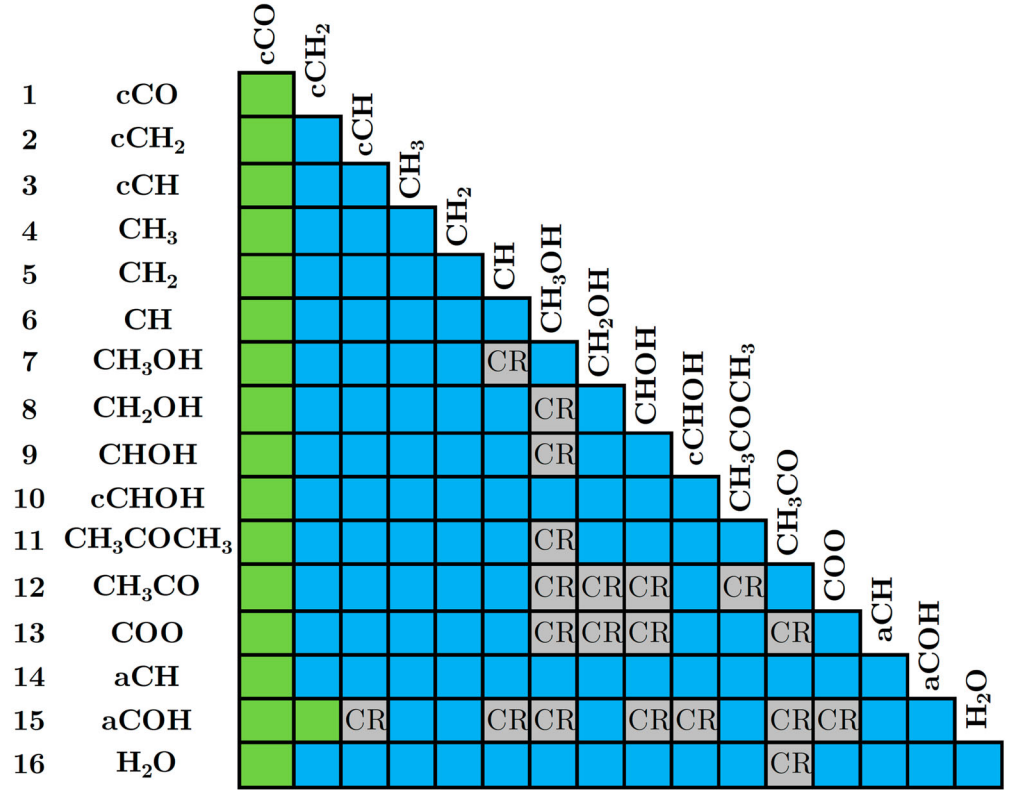

Notes: The interactions for which parameters have been estimated in previous work [4–7, 13–15, 17, 21, 135–137] are denoted by the blue shading. The interactions for which newly estimated parameters are developed in our current work are denoted by the green shading. The grey shading denotes unlike interactions for which parameters have not been refined, and are calculated using combining rules (CR) [4].

Table 4. SAFT-γ Mie group like parameters characterised in the current work.

k	group	v_k^*	S_k	σ_{kk} / Å	λ_{kk}^r	λ_{kk}^a	(ε_{kk}/k_B) / K	$N_{ST,k}$	$n_{k,H}$	n_{k,e_1}	n_{k,e_2}
1	cCO	2	0.52311	2.9769	8.0000	6.0000	477.98	2	–	2	–

The like interaction parameters optimised for cCO are ε_{cCO}, σ_{cCO}, and S_{cCO}, along with the unlike interaction parameters $\varepsilon_{cCO-cCH_2}$ and $\lambda^r_{cCO-cCH_2}$. λ^a_{cCO} is set to 6.0000 as for the other functional groups; this has been shown to be an appropriate value for various molecules, following the work of London [154]. The repulsive exponent of cCO group, λ^r_{cCO} is set to 8.0000 in order to obtain a reasonable value for ε_{cCO}/k_B within the bounds, 50.000 K to 600.00 K. This parameter range reflects the polar nature of the cyclic ketones, which could also be

Table 5. SAFT-γ Mie unlike group parameters (excluding association) characterised in our current work.

k	l	group k	group l	(ε_{kl}/k_B) / K	λ^r_{kl}
1	1	cCO	cCO	477.98	8.0000
1	2	cCO	cCH_2	383.29	14.939
1	3	cCO	cCH	250.81	CR
1	4	cCO	CH_3	264.18	CR
1	5	cCO	CH_2	368.09	CR
1	6	cCO	CH	196.23	CR
1	7	cCO	CH_3OH	338.16	CR
1	8	cCO	CH_2OH	401.70	CR
1	9	cCO	CHOH	289.34	CR
1	10	cCO	cCHOH	299.17	CR
1	11	cCO	CH_3COCH_3	305.47	CR
1	12	cCO	CH_3CO	512.96	CR
1	13	cCO	COO	708.97	CR
1	14	cCO	aCH	392.49	CR
1	15	cCO	aCOH	611.49	CR
1	16	cCO	H_2O	337.62	CR
2	15	cCH2	aCOH	495.01	CR

modelled using e_1 and H sites on the group as for the SAFT-γ Mie model of acetone [5].

The calculated vapour pressure, isobaric density, saturated-liquid and saturated-vapour densities, heat capacity of the saturated liquid, and enthalpy of vaporisation are presented in Figure 2. At a given temperature, the heat capacity and enthalpy of vaporisation increase as the ring size of the cyclic ketones increases, while as expected, the opposite behaviour is found in terms of the vapour pressure. The SAFT-γ Mie calculations are in good qualitative and quantitative agreement with the experimental data as shown in Figure 2 and by the low %AAD values reported in Table 7. It is important to emphasise that this demonstrates the suitability of this approach for the prediction of the properties of four- to eight-membered ring compounds with a unique set of group parameters, showcasing the robustness of the model in capturing the effect of ring size on the thermophysical properties of cyclic compounds.

The SAFT-γ Mie calculations along with the experimental data for cyclic ketones + cyclic alkanes mixtures are presented in Figure 3. As is apparent from the figure, the experimental excess-enthalpy data present a maximum at $x_1^{\text{exp.}} = 0.450$ for cyclohexanone (1) + cyclohexane (2). The SAFT-γ Mie calculations follow a more-symmetrical behaviour with the highest $\Delta h_{\text{mix}} = 0.9\,\text{kJ mol}^{-1}$ at $x_1^{\text{calc.}} = 0.506$ for the same mixture. The isothermal and isobaric VLE experimental data and theoretical calculations show no azeotropic behaviour and are in excellent agreement with each other. Isobaric liquid-density data at $T = 298.15\,\text{K}$, 303.15 K, and 308.15 K, demonstrate linear behaviour with changing composition and T, which is reproduced well by the theoretical calculations.

The AAD and %AAD calculations of the properties of pure cyclic ketones and cyclic ketones + cyclic alkanes mixtures are presented in Table 7. The %AADs for pure cyclic ketones are within 6.672% for the critical temperature, and 32.29% for the vapour pressure. It is worth noting that this larger value is due to the very low vapour-pressure data available for cyclobutanone ($\sim$6 kPa). The model delivers a %AAD within approximately 6% for the other ketones, more in line with the expected performance of SAFT-γ Mie models [14]. In these cases, the AAD is a more-suitable quantity with which to compare the quality of agreement between the SAFT-γ Mie calculations and these experimental data. The AAD value for the vapour pressure of cyclobutanone is only 1.04 kPa, well within the range for AAD values for other cyclic ketones considered in this work, which as can be seen goes up to 27.12 kPa for cyclohexanone. For the cyclic ketones, the %AADs are within 7.163% for the liquid density, 6.758% for the isobaric heat capacity, and 6.816% for the vaporisation enthalpy, respectively. The %AAD values for binary mixtures of cyclohexanone with cyclic alkanes are within 19.19% for the liquid excess enthalpy (corresponding to a small $0.130\,\text{kJ mol}^{-1}$ of AAD), 3.134% for the isothermal VLE, 0.304% for the isobaric VLE, and 0.506% for the liquid density, respectively.

To test the robustness of the model for mixtures of the larger cyclic ketones and transferability of the parameters developed, liquid excess-enthalpies for cyclopentanone, cycloheptanone, and cyclooctanone with cyclopentane and with cyclohexane are also calculated. The agreement of the theoretical calculations with the experimental data available is excellent, confirmed by the low AAD values (within $0.229\,\text{kJ mol}^{-1}$) presented in Table 7.

3.2. Cyclic ketone + primary alcohol mixtures: cCO–CH_3OH and cCO–CH_2OH interactions

The SAFT-γ Mie model for methanol consists of a single CH_3OH molecular group that is composed of two fused segments. [5] This group has three association sites (two e_1 sites and one H site). Ethanol is modelled with one CH_3 group [4] and one CH_2OH group. [13] The CH_2OH group, consisting of two fused Mie segments, also features two e_1 sites and one H site. 1-Propanol to 1-decanol are modelled with one CH_3 group, one CH_2OH group, and one to eight CH_2 group(s), respectively.

To model binary mixtures of cyclic ketones + methanol, experimental data for the methanol + cyclohexanone mixture are considered to characterise the unlike interaction parameters $\varepsilon_{CH_3OH-cCO}$, $\varepsilon^{HB}_{CH_3OH-cCO,H-e_1}$, and $K^{HB}_{CH_3OH-cCO,H-e_1}$. We consider the liquid excess-enthalpy data [87] at $T = 298.15\,\text{K}$

Table 6. SAFT-γ Mie group association parameters developed in our current work.

k	l	group k	site a of group k	group l	site b of group l	$(\varepsilon^{HB}_{kl,ab}/k_B)$ / K	$K^{HB}_{kl,ab}$ / Å^3
1	7	cCO	e_1	CH_3OH	H	1500.0	341.83
1	8	cCO	e_1	CH_2OH	H	1397.1	320.81
1	9	cCO	e_1	CHOH	H	2498.8	44.784
1	10	cCO	e_1	cCHOH	H	1474.8	534.94
1	11	cCO	e_1	CH_3COCH_3	H	936.25	1955.5
1	15	cCO	e_1	aCOH	H	2909.7	15.928
1	16	cCO	e_1	H_2O	H	1656.3	163.09

and $P = 101.3$ kPa and the isobaric VLE data [89] at $P = 94.80$ kPa for cyclohexanone + methanol. Liquid-density data [92] at $T = 293.15$ K and $P = 101.3$ kPa for cyclohexanone + methanol and liquid excess enthalpy data [95] at $T = 298.15$ K and $P = 101.3$ kPa for cyclopentanone + methanol data are also available, which allows us to assess the transferability of the parameters optimised.

To model mixtures of cyclic ketones with other primary alcohols (from ethanol to 1-decanol), experimental data for ethanol + cyclohexanone and 1-propanol + cyclopentanone are considered to refine the unlike interaction parameters $\varepsilon_{CH_2OH-cCO}$, $\varepsilon^{HB}_{CH_2OH-cCO,H-e_1}$, and $K^{HB}_{CH_2OH-cCO,H-e_1}$. In particular, we consider the isobaric VLE experimental data [88] at $P = 101.3$ kPa for ethanol + cyclohexanone and the liquid excess-enthalpy data [95] at $T = 298.15$ K and $P = 101.3$ kPa for 1-propanol + cyclopentanone. Liquid excess-enthalpy data [87, 95] for ethanol to 1-pentanol with cyclohexanone and with cyclopentanone, isobaric VLE data [88, 89, 91, 96, 97, 109] for ethanol, 1-butanol, 1-pentanol with cyclohexanone and with cyclopentanone, liquid-density data [92, 93, 98] for ethanol to 1-decanol with cyclohexanone and propanol to 1-hexanol with cyclopentanone data are also available; these data are used to test the transferability of the optimised parameters. The SAFT-γ Mie calculations are compared with these experimental data for binary mixtures of primary alcohols with cyclohexanone and with cyclopentanone in Figures 4 and 5.

In Figure 4(a), a positive deviation is observed for all the mixtures including primary alcohols considered at $P = 101.3$ kPa with the highest $\Delta h_{mix} = 1.754$ kJ mol^{-1} at $x_1^{calc.} = 0.576$ for cyclohexanone (1) + 1-decanol (2). No azeotropic VLE behaviour is observed experimentally or theoretically for any of the mixtures considered. For the liquid density, non-ideal behaviour is observed. Mixtures including short-chain primary alcohols exhibit concave-shaped density curves. Almost-ideal behaviour is observed for 1-pentanol + cyclohexanone and 1-propanol + cyclopentanone. Finally, convex-shaped curves are obtained for mixtures including longer primary alcohols. The order of increasing mixture density changes for binary mixtures including primary alcohols and cyclic ketones at a crossover molar fraction roughly at $x_1 = 0.20$ for cyclohexanone (1) and at $x_1 = 0.22$ for cyclopentanone (1).

Excellent agreement is obtained between the experimental data and the theoretical calculations, reflected in the low %AAD values reported in Table 7. The %AAD values are within 14.41% for the liquid excess enthalpy (with a low 0.135 kJ mol^{-1} AAD), 0.444% for the isobaric VLE, and 2.133% for the liquid density of mixtures of primary alcohols with cyclopentanone and with cyclohexanone.

3.3. Cyclic ketone + cyclic alcohol mixtures: cCO–cCHOH interactions

To model cyclic alcohols with SAFT-γ Mie, the cCHOH group was developed in recent work [17]. In our current work, we use experimental data for cyclohexanone + cyclohexanol to characterise the unlike interaction parameters $\varepsilon_{cCHOH-cCO}$, $\varepsilon^{HB}_{cCHOH-cCO,H-e_1}$, and $K^{HB}_{cCHOH-cCO,H-e_1}$. We consider the liquid excess-enthalpy data [99] at $T = 303.15$ K and $P = 101.3$ kPa, and the isothermal VLE data [104] at $T = 373.15$ K and 383.15 K. Liquid excess-enthalpy data [100] at $T = 298.15$ K and $P = 101.3$ kPa for cyclopentanol + cyclohexanone, isobaric VLE data [101, 102] at $P =$ 26.67 kPa, 52.66 kPa and 100.8 kPa, isothermal VLE data [103, 104] at $T = 323.15$ K and 343.15 K, and liquid-density data [106] at $x_1 = 0.63$ and $P = 101.3$ kPa for cyclohexanone (1) + cyclohexanol (2) are also available, and are used to assess the quality of the optimised parameters. SAFT-γ Mie calculations are compared with these experimental data in Figure 6.

As can be seen in Figure 6(a), the excess-enthalpy data are positive and close to symmetric, with a maximum $\Delta h_{mix}^{calc.} = 1.429$ kJ mol^{-1} at $x_1^{calc.} = 0.506$ for cyclohexanone (1) + cyclohexanol (2). Furthermore, narrow isobaric and isothermal VLE regions are obtained for this mixture (cf. Figure 6(b,c)). For the higher-pressure and lower-temperature ranges, the vapour-pressure values of the two compounds are close to each other, leading to an isobaric and isothermal azeotropic VLE behaviour from $P = 100.8$ kPa and $T = 343.15$ K onwards, respectively.

Table 7. Overview of the accuracy of SAFT-γ Mie in the calculation of pure fluid and binary mixture properties: critical temperature, vapour pressure, isobaric liquid density, saturated-liquid density, isobaric heat capacity of the saturated liquid, enthalpy of vaporisation, bubble temperature, dew temperature, bubble pressure, dew pressure, LLE composition, SLE composition (solubility), mixture density, and excess molar enthalpy.

Critical temperature

System s (pure)	T / K	P	x_1	$N_{s,p}^{est.}$	$N_{s,p}^{tot.}$	%AAD$_{s,p}$	AAD$_{s,p}$ / K	Ref.	Fig.
cyclobutanone	631.5	critical	pure	0	1	6.672	39.50	[134]	2
cyclopentanone	644	critical	pure	0	1	3.122	19.50	[134]	2
cyclohexanone	661	critical	pure	0	1	0.587	3.900	[134]	2
cycloheptanone	680	critical	pure	0	1	0.741	5.000	[134]	2
cyclooctanone	698.5	critical	pure	0	1	1.481	10.50	[134]	2
3-methylcyclohexanone	671	critical	pure	0	1	2.287	15.00	[134]	8
menthone	696	critical	pure	0	1	9.124	63.50	[134]	8

Vapour pressure

System s (pure)	T / K	P	x_1	$N_{s,p}^{est.}$	$N_{s,p}^{tot.}$	%AAD$_{s,p}$	AAD$_{s,p}$ / kPa	Ref.	Fig.
cyclobutanone	249–298	saturation	pure	0	11	32.29	1.040	[138]	2
cyclopentanone	323–403	saturation	pure	15	15	2.097	1.188	[142]	2
cyclohexanone	394–575	saturation	pure	17	17	3.419	27.12	[139, 140]	2
cycloheptanone	373–464	saturation	pure	0	19	6.109	3.712	[141]	2
cyclooctanone	394–484	saturation	pure	0	13	2.731	2.559	[141]	2
3-methylcyclohexanone	334–441	saturation	pure	0	21	5.676	1.113	[73]	8
menthone	280–696	saturation	pure	0	29	65.96	233.5	[134, 155–161]	8

Liquid density

System s (pure)	T / K	P / kPa	x_1	$N_{s,p}^{est.}$	$N_{s,p}^{tot.}$	%AAD$_{s,p}$	AAD$_{s,p}$ / (kg m^{-3})	Ref.	Fig.
cyclobutanone	293–362	101.3	pure	0	10	7.163	64.11	[141]	2
cyclopentanone	243–593	saturation	pure	9	21	1.530	12.72	[144, 145]	2
cyclohexanone	253–613	saturation	pure	18	25	2.061	15.29	[143, 146]	2
cycloheptanone	297–373	101.3	pure	0	7	3.147	28.72	[141]	2
cyclooctanone	316–411	101.3	pure	0	9	4.566	40.74	[141]	2
3-methylcyclohexanone	280–656	saturation	pure	0	26	4.266	23.20	[134]	8
	293–360	101.3	pure	0	5	1.986	17.53	[163]	8
menthone	292–453	saturation	pure	0	12	1.556	13.09	[162]	8

Molar heat capacity

System s (pure)	T / K	P / kPa	x_1	$N_{s,p}^{est.}$	$N_{s,p}^{tot.}$	%AAD$_{s,p}$	AAD$_{s,p}$ / (J mol^{-1} K^{-1})	Ref.	Fig.
cyclopentanone	217–327	101.3	pure	0	29	6.758	9.974	[63]	2
cyclohexanone	245–301	101.3	pure	0	24	2.858	4.802	[147]	2
cycloheptanone	293–308	101.3	pure	0	4	2.463	4.986	[148]	2
3-methylcyclohexanone	280–640	saturation	pure	0	19	2.537	8.031	[164]	8
menthone	260–640	saturation	pure	0	19	1.783	7.119	[164]	8

Vaporisation enthalpy

System s (pure)	T / K	P	x_1	$N_{s,p}^{est.}$	$N_{s,p}^{tot.}$	%AAD$_{s,p}$	AAD$_{s,p}$ / (kJ mol^{-1})	Ref.	Fig.
cyclopentanone	243–593	saturation	pure	0	11	2.073	0.546	[144]	2
cyclohexanone	253–603	saturation	pure	0	11	6.816	2.008	[144]	2
cycloheptanone	298	saturation	pure	0	1	1.628	0.824	[149]	2
cyclooctanone	298	saturation	pure	0	1	5.032	2.694	[149]	2
3-methylcyclohexanone	280–640	saturation	pure	0	19	8.728	2.403	[165]	8
menthone	255–680	saturation	pure	0	21	25.67	9.072	[165]	8

T–x diagram

System s (1+2)	T	P / kPa	x_1	$N_{s,p}^{est.}$	$N_{s,p}^{tot.}$	%AAD$_{s,p}$	AAD$_{s,p}$ / K	Ref.	Fig.
cyclohexanone + cyclohexane	T_{bub}	101.3	0.067–0.985	0	21	0.304	1.131	[151]	3
	T_{dew}	101.3	0.019–0.84	0	21	0.556	2.064	[151]	3
cyclohexanone + 3-methylcyclohexanone	T_{bub}	13.33–26.66	0–1	15	32	0.513	1.995	[74, 75]	N/A
	T_{dew}	13.33–26.66	0–1	0	32	0.529	1.669	[74, 75]	N/A
cyclohexanone + 1-decane	T_{bub}	95.80	0–1	0	7	0.571	2.456	[83]	N/A
cyclohexanone + methanol	T_{bub}	94.80	0–1	8	8	0.444	1.603	[89]	4
cyclohexanone + ethanol	T_{bub}	101.3	0–1	16	16	0.208	0.7929	[88]	4
	T_{dew}	101.3	0–1	16	16	0.206	0.813	[88]	4
cyclohexanone + 1-butanol	T_{bub}	101.3	0.044–0.954	0	9	0.189	0.768	[90]	4
	T_{dew}	101.3	0.0353–0.8243	0	9	0.162	0.647	[90]	4
cyclohexanone + 1-pentanol	T_{bub}	101.3	0–1	0	12	0.114	0.482	[91]	4
	T_{dew}	101.3	0–1	0	12	0.102	0.428	[91]	4
cyclopentanone + ethanol	T_{bub}	101.3	0–1	0	14	0.283	1.061	[96]	5

(*continued*).

Table 7. Continued.

T–x diagram									
System *s* (pure)	*T* / K	*P*	x_1	$N_{s,p}^{est.}$	$N_{s,p}^{tot.}$	%AAD$_{s,p}$	AAD$_{s,p}$ / K	Ref.	Fig.
	T_{dew}	101.3	0–1	0	14	0.134	0.520	[96]	5
cyclopentanone + 1-butanol	T_{bub}	101.3	0.1003–0.9	0	9	0.195	0.765	[97]	5
cyclopentanone + 1-pentanol	T_{bub}	101.3	0.1–0.8943	0	9	0.145	0.588	[97]	5
cyclohexanone + 2-propanol	T_{bub}	101.3	0–1	16	16	0.164	0.641	[88]	N/A
	T_{dew}	101.3	0–1	0	16	0.232	0.920	[88]	N/A
cyclohexanone + 2-butanol	T_{bub}	94.80	0–1	0	8	0.429	1.697	[89]	N/A
cyclohexanone + isobutanol	T_{bub}	94.80	0.3891–1	0	5	0.151	0.617	[89]	N/A
cyclohexanone + isopentanol	T_{bub}	101.3	0.098–0.9024	0	9	0.597	2.452	[97]	N/A
cyclopentanone + isopentanol	T_{bub}	101.3	0.1004–0.899	0	9	0.285	1.146	[97]	N/A
cyclohexanone + cyclohexanol	T_{bub}	26.66-100.8	0–1	0	23	0.191	0.803	[101, 102]	6
	T_{dew}	26.66-100.8	0–1	0	23	0.221	0.925	[101, 102]	6
cyclohexanone + 2-propanone	T_{bub}	101.3	0.1083–0.897	9	9	0.270	1.001	[109]	N/A
cyclohexanone + 2-butanone	T_{bub}	101.3	0.011–0.9312	0	18	0.679	2.628	[109]	N/A
	T_{dew}	101.3	0.011–0.449	0	9	0.496	1.883	[109, 110]	N/A
cyclopentanone + 2-butanone	T_{bub}	101.3	0-1	0	13	0.113	0.410	[113]	N/A
	T_{dew}	101.3	0–1	0	13	0.140	0.512	[113]	N/A
cyclohexanone + benzene	T_{bub}	101.3	0.1106–0.9682	5	14	1.625	6.257	[122]	N/A
	T_{dew}	101.3	0.0115–0.8621	5	14	0.789	2.950	[122]	N/A
cyclohexanone + phenol	T_{bub}	11.99–101.3	0–1	22	50	0.198	0.816	[126–129]	N/A
	T_{dew}	11.99–101.3	0–1	22	36	0.171	0.715	[126, 127, 129]	N/A
cyclopentanone + water	T_{bub}	101.3	0–1	0	22	0.537	2.039	[132]	7
	T_{dew}	101.3	0–1	0	22	0.342	1.298	[132]	7
cyclohexanone + water	T_{bub}	101.3	0.0028–1	0	7	0.349	1.349	[104]	7
	T_{dew}	101.3	0.0129–1	0	7	0.812	3.123	[104]	7
menthone + menthol	T_{bub}	23.99	0.114–0.902	0	9	7.649	33.03	[157]	9
	T_{dew}	23.99	0.183–0.935	0	9	7.660	33.08	[157]	9
P–x diagram									
System *s* (1+2)	*T* / K	*P*	x_1	$N_{s,p}^{est.}$	$N_{s,p}^{tot.}$	%AAD$_{s,p}$	AAD$_{s,p}$ / kPa	Ref.	Fig.
cyclohexanone + cyclohexane	348	P_{bub}	0.04–0.935	14	14	3.134	1.807	[152]	3
	348	P_{dew}	0.0095–0.338	14	14	1.376	0.749	[152]	3
cyclopentanone + cyclohexane	313	P_{bub}	0.0929–1	0	32	9.014	1.241	[72]	N/A
	313	P_{dew}	0.0477–1	0	32	2.912	0.632	[72]	N/A
cyclopentanone + 1-hexane	313	P_{bub}	0.0294–0.8126	0	13	4.595	1.356	[72]	N/A
	313	P_{dew}	0.0294–0.8126	0	13	6.004	1.897	[72]	N/A
cyclohexanone + cyclohexanol	323–383	P_{bub}	0–1	10	56	7.868	0.184	[103, 105]	6
	323–383	P_{dew}	0–1	0	15	4.527	0.393	[105]	6
cyclohexanone + 2-heptanone	313–393	P_{bub}	0–1	0	87	60.76	6.510	[114]	N/A
cyclohexanone + ethyl acetate	293	P_{bub}	0–1	0	9	12.92	0.891	[118, 134]	N/A
cyclopentanone + benzene	313	P_{bub}	0.1027–0.9445	0	12	15.96	1.833	[72]	N/A
	313	P_{dew}	0.0231–0.7511	0	12	15.50	2.295	[72]	N/A
cyclohexane + phenol	323–363	P_{bub}	0.0155–0.064	0	16	16.92	3.231	[125]	N/A
cyclohexanone + phenol	378–423	P_{bub}	0–1	0	28	5.476	1.328	[127]	N/A
cyclohexanone + water	363	P_{bub}	0.0025–0.96	14	14	5.757	3.173	[104]	7
	363	P_{dew}	0.041–0.368	14	14	2.474	1.653	[104]	7
Composition									
System *s* (1+2)	*T* / K	*P* / kPa	x_1	$N_{s,p}^{est.}$	$N_{s,p}^{tot.}$	%AAD$_{s,p}$	AAD$_{s,p}$ / (mol.mol^{-1})	Ref.	Fig.
cyclohexanone + 2-pentanone	184–241	101.3	x_1^{sat}	0	11	18.01	0.044	[111]	N/A
cyclopentanone + 2-propanone	168–203	101.3	x_1^{sat}	0	9	61.33	0.271	[112]	N/A
cyclopentanone + 2-pentanone	188–198	101.3	x_1^{sat}	0	3	24.15	0.126	[112]	N/A
cyclohexane + phenol	279–314	101.3	x_1^{sat}	0	15	28.52	0.097	[123]	N/A
cyclopentanone + water	266–272	101.3	x_1^{sat}	0	9	15.22	0.020	[133]	7
	273–363	101.3	x_1^{LLE}	10	10	9.709	0.023	[131]	7
cyclohexanone + water	273–363	101.3	x_1^{LLE}	0	10	14.85	0.015	[131]	7
cycloheptanone + water	273–365	101.3	x_1^{LLE}	0	10	28.42	0.018	[131]	7
menthone + menthol	261–312	101.3	x_1^{sat}	0	8	6.971	0.038	[166]	9
menthone + water	298–313	101.3	x_1^{LLE}	0	2	41.72	9.1×10^{-6}	[55]	9
Density of binary mixture									
System *s* (1+2)	*T* / K	*P* / kPa	x_1	$N_{s,p}^{est.}$	$N_{s,p}^{tot.}$	%AAD$_{s,p}$	AAD$_{s,p}$ / (kg m^{-3})	Ref.	Fig.
cyclohexanone + cyclohexane	298–308	101.3	0–1	22	33	0.506	9.072	[153]	3
cyclohexanone + methylcyclohexane	303	101.3	0–1	0	8	0.694	5.860	[77]	N/A
cyclohexanone + 1-hexane	298	101.3	0–1	11	11	0.320	2.572	[79]	N/A
cyclohexanone + 1-heptane	298	101.3	0–1	0	11	0.338	2.710	[79]	N/A

(*continued*).

Table 7. Continued.

Density of binary mixture									
System *s* (pure)	*T* / K	*P*	x_1	$N_{s,p}^{est.}$	$N_{s,p}^{tot.}$	%AAD$_{s,p}$	AAD$_{s,p}$ / K	Ref.	Fig.
cyclohexanone + methanol	293	101.3	0–1	0	14	1.075	9.677	[92]	4
cyclohexanone + ethanol	298	101.3	0–1	0	11	1.065	9.409	[93]	4
cyclohexanone + 1-butanol	298	101.3	0–1	0	11	0.795	7.006	[93]	4
cyclohexanone + 1-pentanol	298	101.3	0–1	0	12	0.715	6.102	[93]	4
cyclohexanone + 1-hexanol	298	101.3	0–1	0	11	0.624	5.404	[93]	4
cyclohexanone + 1-octanol	298	101.3	0–1	0	11	0.615	5.329	[93]	4
cyclohexanone + 1-decanol	298	101.3	0–1	0	11	0.659	5.699	[93]	4
cyclopentanone + 1-propanol	303	101.3	0.1172–0.9115	0	6	2.133	18.58	[98]	5
cyclopentanone + 1-butanol	303	101.3	0.1039–0.9018	0	6	1.525	13.26	[98]	5
cyclopentanone + 1-pentanol	303	101.3	0.0926–0.8818	0	6	1.118	9.670	[98]	5
cyclopentanone + 1-hexanol	303	101.3	0.0722–0.8682	0	6	0.753	6.468	[98]	5
cyclohexanone + isopentanol	298	101.3	0–1	0	11	0.778	6.629	[94]	N/A
cyclopentanone + isopentanol	298	101.3	0–1	0	12	1.464	12.62	[94]	N/A
cyclohexanone + cyclohexanol	303–430	101.3	0.63	0	21	0.803	6.854	[106]	6
cyclohexanone + 2-propanone	293	101.3	0.1481–0.7499	0	4	0.273	2.424	[115]	N/A
cyclohexanone + 2-butanone	298	101.3	0–1	0	22	0.486	4.313	[116]	N/A
cyclopentanone + hexyl acetate	298	101.3	0.015–0.234	0	10	0.148	1.296	[119]	N/A
cyclohexanone + benzene	298	101.3	0–1	0	12	1.535	13.93	[79]	N/A
cyclohexane + phenol	303	101.3	0–1	0	9	0.601	5.429	[124]	N/A
Excess molar enthalpy									
System *s* (1+2)	*T* / K	*P* / kPa	x_1	$N_{s,p}^{est.}$	$N_{s,p}^{tot.}$	%AAD$_{s,p}$	AAD$_{s,p}$ / (kJ mol^{-1})	Ref.	Fig.
cyclohexanone + cyclopentane	298	101.3	0.0651–0.9371	0	18	19.19	0.130	[78]	3
cyclohexanone + cyclohexane	298	101.3	0.025–0.975	9	21	13.81	0.067	[150]	3
cyclopentanone + cyclopentane	298	101.3	0.1165–0.8219	0	10	13.50	0.103	[71]	N/A
cyclopentanone + cyclohexane	298	101.3	0.1079–0.8963	0	13	15.39	0.124	[71]	N/A
cycloheptanone + cyclopentane	298	101.3	0.1968–0.7646	0	9	18.21	0.115	[71]	N/A
cycloheptanone + cyclohexane	298	101.3	0.1144–0.8059	0	12	19.29	0.135	[71]	N/A
cyclooctanone + cyclopentane	313	101.3	0.1969–0.8097	0	8	38.96	0.229	[71]	N/A
cyclooctanone + cyclohexane	313	101.3	0.163–0.8167	0	10	33.91	0.227	[71]	N/A
cyclohexanone + methylcyclohexane	298	101.3	0.0376–0.972	0	21	74.55	0.522	[76]	N/A
cyclohexanone + 1-pentane	298	101.3	0.0787–0.90449	0	12	18.26	0.121	[78]	N/A
cyclohexanone + 1-hexane	298	101.3	0.0801–0.92085	10	13	12.59	0.092	[78]	N/A
cyclohexanone + 1-heptane	298	101.3	0.1241–0.9341	0	12	11.16	0.098	[80]	N/A
cyclohexanone + 1-octane	298	101.3	0.1304–0.9115	0	10	16.44	0.133	[81]	N/A
cyclohexanone + 1-nonane	298	101.3	0.0565–0.9492	0	15	18.42	0.138	[82]	N/A
cyclohexanone + 1-decane	298	101.3	0.1014–0.8715	0	10	10.03	0.095	[81]	N/A
cyclopentanone + 1-pentane	298	101.3	0.958–0.99	0	5	15.87	0.022	[84]	N/A
cyclopentanone + 1-hexane	298	101.3	0.021–0.982	0	17	21.27	0.122	[84]	N/A
cyclopentanone + 1-heptane	298	101.3	0.11–0.8949	0	10	13.83	0.139	[85]	N/A
cyclopentanone + 1-octane	298	101.3	0.1022–0.8905	0	10	27.25	0.248	[81]	N/A
cyclopentanone + 1-nonane	298	101.3	0.0348–0.9545	0	16	30.21	0.265	[82]	N/A
cyclopentanone + 1-decane	298	101.3	0.0979–0.8907	0	10	30.62	0.306	[81]	N/A
cycloheptanone + 1-nonane	298	101.3	0.0572–0.9547	0	14	12.81	0.086	[82]	N/A
cyclohexanone + methanol	298	101.3	0.043–0.9014	9	21	3.712	0.013	[87]	4
cyclohexanone + ethanol	298	101.3	0.0433–0.9242	0	26	2.357	0.021	[87]	4
cyclohexanone + 1-propanol	298	101.3	0.0906–0.9094	0	21	2.737	0.025	[87]	4
cyclohexanone + 1-butanol	298	101.3	0.0587–0.9332	0	19	3.979	0.034	[87]	4
cyclohexanone + 1-pentanol	298	101.3	0.0571–0.9071	0	118	6.527	0.062	[87]	4
cyclopentanone + methanol	298	101.3	0.09–0.9071	0	10	14.41	0.082	[95]	5
cyclopentanone + ethanol	298	101.3	0.0899–0.9055	0	10	4.733	0.042	[95]	5
cyclopentanone + 1-propanol	298	101.3	0.0902–0.9102	10	10	1.744	0.019	[95]	5
cyclopentanone + 1-butanol	298	101.3	0.0899–0.9107	0	10	10.38	0.118	[95]	5
cyclopentanone + 1-pentanol	298	101.3	0.0898–0.9103	0	10	13.16	0.135	[95]	5
cyclohexanone + 2-propanol	298	101.3	0.0587–0.9157	8	12	1.174	0.010	[86]	N/A
cyclohexanone + isobutanol	298	101.3	0.0573–0.9247	10	12	6.146	0.049	[86]	N/A
cyclohexanone + cyclohexanol	303	101.3	0.2245–0.7563	14	14	1.993	0.022	[99]	6
cyclohexanone + cyclopentanol	298	101.3	0.0866–0.9181	0	10	9.745	0.108	[100]	6
cyclohexanone + 2-propanone	298	101.3	0.1292–0.9068	1	18	90.58	0.080	[107]	N/A
cyclohexanone + 2-butanone	298	101.3	0.025–0.975	15	21	17.75	0.006	[108]	N/A
cyclopentanone + 2-propanone	298	101.3	0.136–0.9074	0	18	645.1	0.218	[107]	N/A
cycloheptanone + 2-propanone	298	101.3	0.1234–0.9024	0	18	62.76	0.110	[107]	N/A
cyclohexanone + pentyl acetate	298	101.3	0.206–0.864	11	11	6.716	0.011	[117]	N/A
cyclohexanone + benzene	298	101.3	0.092–0.9252	10	17	2.343	0.005	[121]	N/A
cyclopentanone + benzene	298	101.3	0.0871–0.9128	0	8	9.665	0.022	[85]	N/A
cyclohexane + phenol	313	101.3	0.18–0.86	10	12	14.81	0.143	[123]	N/A
cyclohexanone + water	293–323	101.3	0.011–0.894	6	23	310.4	0.130	[130]	7

Notes: $N_{s,p}^{est}$ is the number of experimental data points used in the parameter estimation, and $N_{s,p}^{tot}$ the number of experimental data points used to calculate %AAD$_{s,p}$ and AAD$_{s,p}$, for system *s* and property *p*.

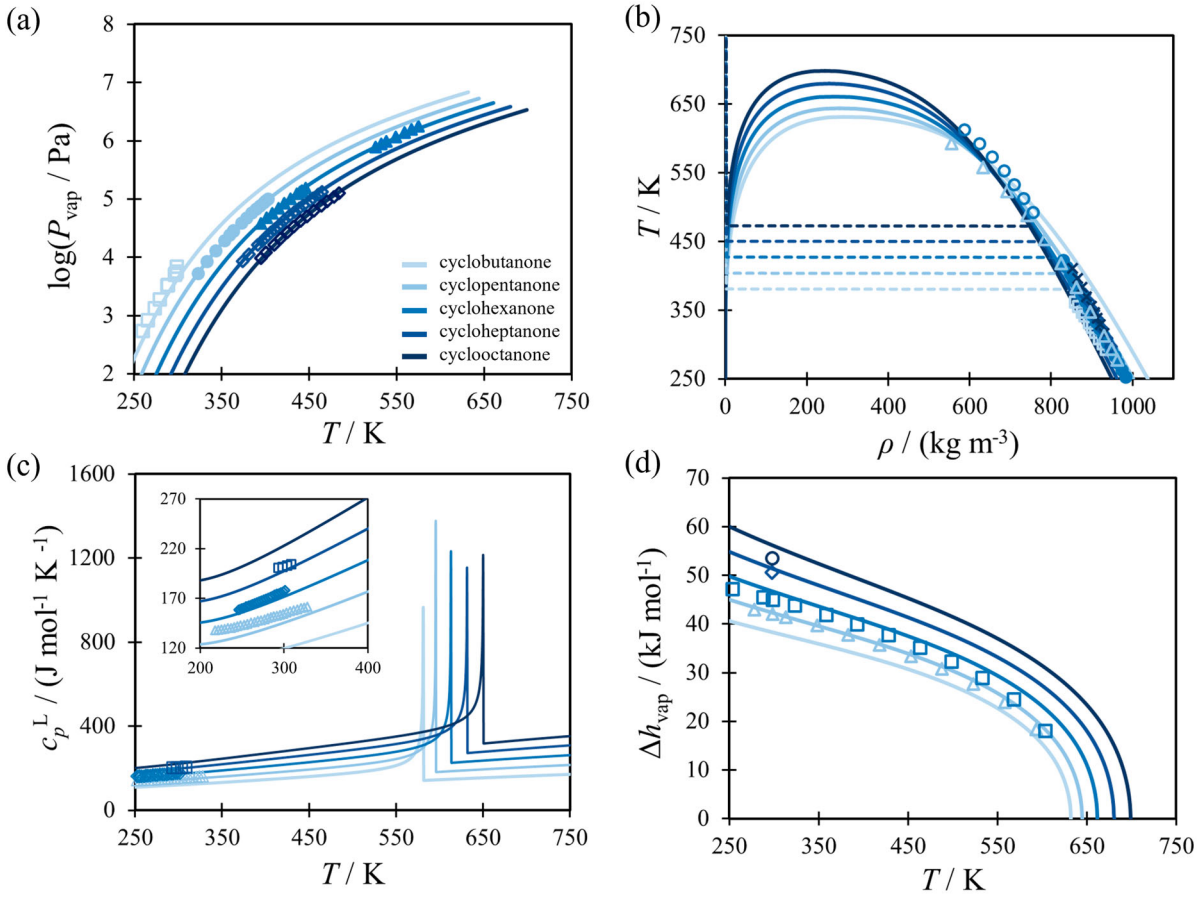

Figure 2. Selected thermodynamic properties of cyclic ketones. The legend in subplot (a) is applicable to all of the subplots. The continuous curves represent the SAFT-γ Mie calculations. The filled symbols [139, 140, 142, 143, 145] represent the experimental data points included in the parameter estimation while the hollow symbols [63, 138, 141, 143, 144, 146–149] represent the data points used in the validation of the theoretical description. (a) Vapour pressure. (b) Temperature–density diagram, saturated density curves are represented with continuous curves and isobaric density calculation curves at 101.3 kPa are represented with dashed curves. (c) Isobaric heat capacity at 101.3 kPa. (d) Enthalpy of vaporisation. The experimental data references corresponding to each pure compound and its property are provided in Table 7.

A quasi-linear curve is obtained for the temperature dependence of the liquid density (Figure 6(d)) at a fixed molar composition of cyclohexanone, $x_1 = 0.63$ and $P = 0.101$ MPa, for cyclohexanone (1) + cyclohexanol (2).

The quantitative agreement between the experimental data and the theoretical calculations is excellent as is apparent from the AAD values reported in Table 7. The %AAD values are within 9.745% for the liquid excess enthalpy (corresponding to 0.108 kJ mol^{-1} AAD), 0.221% for the isobaric VLE, 7.868% for the isothermal VLE, and 0.803% for liquid density.

3.4. Cyclic ketone + water mixtures: cCO–H_2O interactions

In our current work, water is represented with a single spherical Mie segment, using the model of Dufal et al. [6, 7]. We consider the experimental data for binary mixtures of water with cyclopentanone and with cyclohexanone to refine the unlike interaction parameters ε_{H_2O-cCO}, $\varepsilon^{HB}_{H_2O-cCO,H-e_1}$, and $K^{HB}_{H_2O-cCO,H-e_1}$. Liquid excess-enthalpy data [130] at $T = 293.15$ K and $P = 101.3$ kPa, isothermal azeotropic VLE data [104] at $T = 363.15$ K for cyclohexanone + water, and isobaric LLE data [131] at $P = 101.3$ kPa for cyclopentanone + water are considered. Liquid excess-enthalpy data [130] at $T = 308.15$ K and 323.15 K and $P = 101.3$ kPa, isobaric LLE data [131] and isobaric azeotropic VLE data [104] at $P = 101.3$ kPa for cyclohexanone + water, isobaric VLE data, [132] and isobaric SLE data [133] at $P = 101.3$ kPa for cyclopentanone + water, and isobaric LLE data [131] at $P = 101.3$ kPa for cycloheptanone + water are also used to test the transferability of the optimised parameters. The SAFT-γ Mie predictions are compared with these experimental data in Figure 7.

In Figure 7(a), an 'S'-shaped curve can be seen in the experimental excess enthalpy reported for cyclohexanone

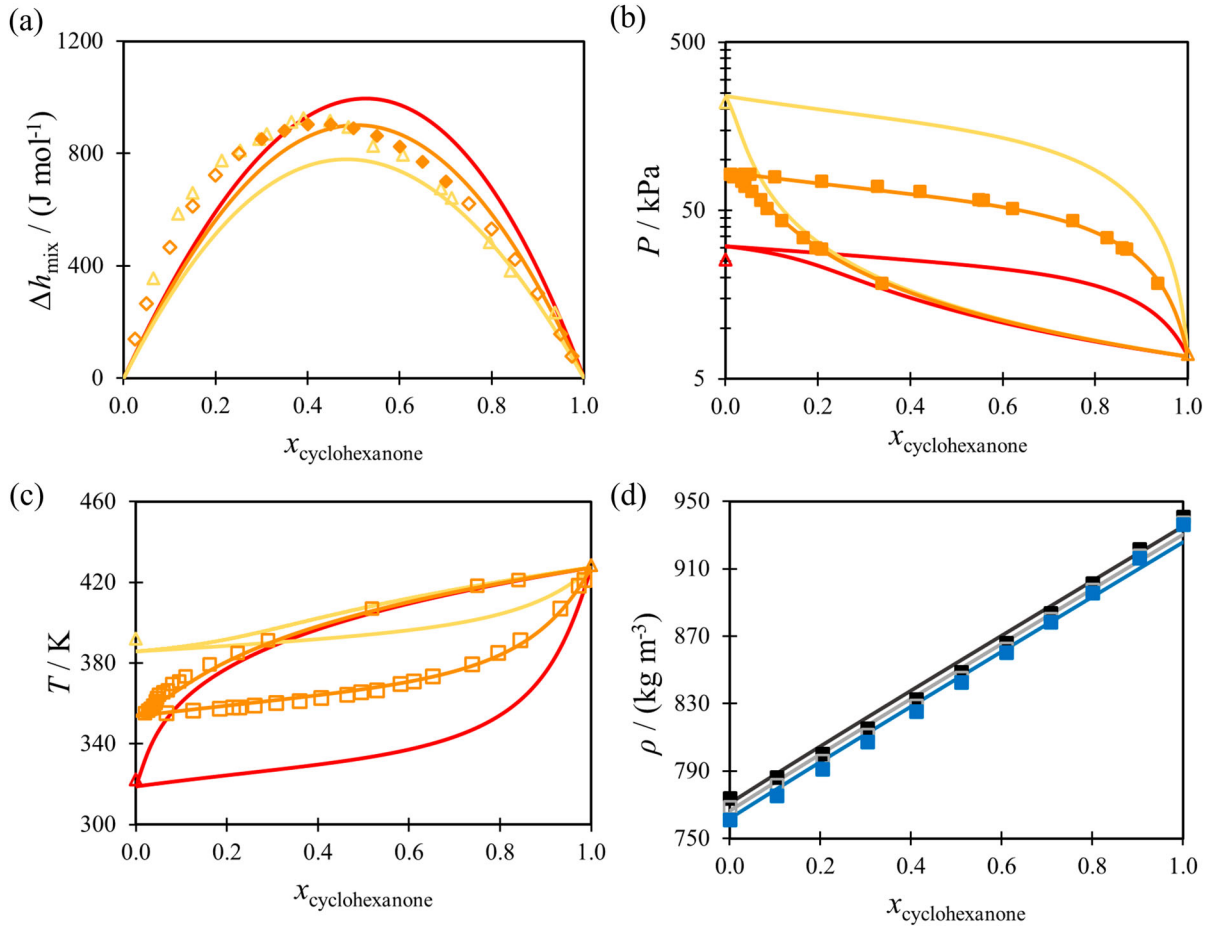

Figure 3. Selected thermodynamic properties of cyclohexanone + cyclic alkane mixtures. The colour index for cyclic alkanes in (a), (b), and (c) is as follows: cyclopentane (yellow), cyclohexane (orange), and cycloheptane (red). The continuous curves represent the SAFT-γ Mie calculations. The filled symbols [150, 152, 153] represent the experimental data points included in the parameter estimation while the hollow symbols [71, 78] represent the data points used in the validation of the theoretical description. (a) Excess enthalpy at atmospheric pressure and $T = 298.15$ K. (b) Isothermal vapour–liquid equilibrium at $T = 348.15$ K. (c) Isobaric vapour–liquid equilibrium at P = 101.3 kPa. (d) Liquid density of cyclohexanone + cyclohexane mixture at atmospheric pressure and $T = 298.15$ K (black), 303.15 K (grey), and 308.15 K (blue). The experimental data references corresponding to each mixture and its property are given in Table 7.

+ water, and in the theoretical calculations, with the minimum $\Delta h_{mix}^{calc.} = -0.220\,kJ\,mol^{-1}$ at $x_1^{calc.} = 0.088$ and maximum $\Delta h_{mix}^{calc.} = 0.510\,kJ\,mol^{-1}$ at $x_1^{calc.} = 0.684$ at $T = 298.15$ K, for cyclohexanone (1) + water (2). As can be seen in Figure 7 (b), the mixture presents azeotropic isothermal vapour–liquid–liquid-equilibrium (VLLE) behaviour at $T = 363.15$ K, which is well reproduced by the SAFT-γ Mie calculations. The LLE region is bounded by the VLLE curve at low pressure ($P^{exp.} = 80.86$ kPa and $P^{calc.} = 76.50$ kPa).

Constant-pressure ($P = 101.3$ kPa), temperature–mole fraction phase diagrams including narrow regions of heteroazeotropic VLLE, LLE, solid–liquid–liquid-equilibrium (SLLE) and solid–solid-liquid-equilibrium (SSLE) eutetic points for binary mixtures of water with cyclopentanone, with cyclohexanone, and with cycloheptanone are presented in Figure 7(c–e). This is a stringent test for the theory as this kind of complex phase behaviour is difficult to capture. For the cyclopentanone + water mixture (Figure 7(c)), the LLE region is bounded by the heteroazeotropic VLLE line at high temperature, $T^{exp.} = 367.8$ K and $T^{calc.} = 366.9$ K, and by the SLLE line at low temperature, $T^{exp.} = 266.1$ K and $T^{calc.} = 264.5$ K. The eutectic point obtained with the theoretical calculation is at $x_{1,eut}^{calc.} = 0.934$. For the cyclohexanone (1) + water (2) mixture (Figure 7(d)), the LLE region is bounded by the heteroazeotropic VLLE line at high temperature, $T^{exp.} = 369.5$ K and $T^{calc.} = 372.0$ K, and by an SLLE line at low temperature, $T^{calc.} = 271.6$ K. The eutectic point obtained from the theoretical calculation is at $x_{1,eut}^{calc.} = 0.949$. For the cycloheptanone (1) + water (2) mixture (Figure 7(e)), the LLE region is bounded by the heteroazeotropic VLLE line at high temperature, $T^{calc.} = 372.0$ K, and by the SLLE line at low temperature, $T^{calc.} = 271.9$ K. The eutectic point obtained theoretically is at $x_{1,eut}^{calc.} = 0.946$. Comparing

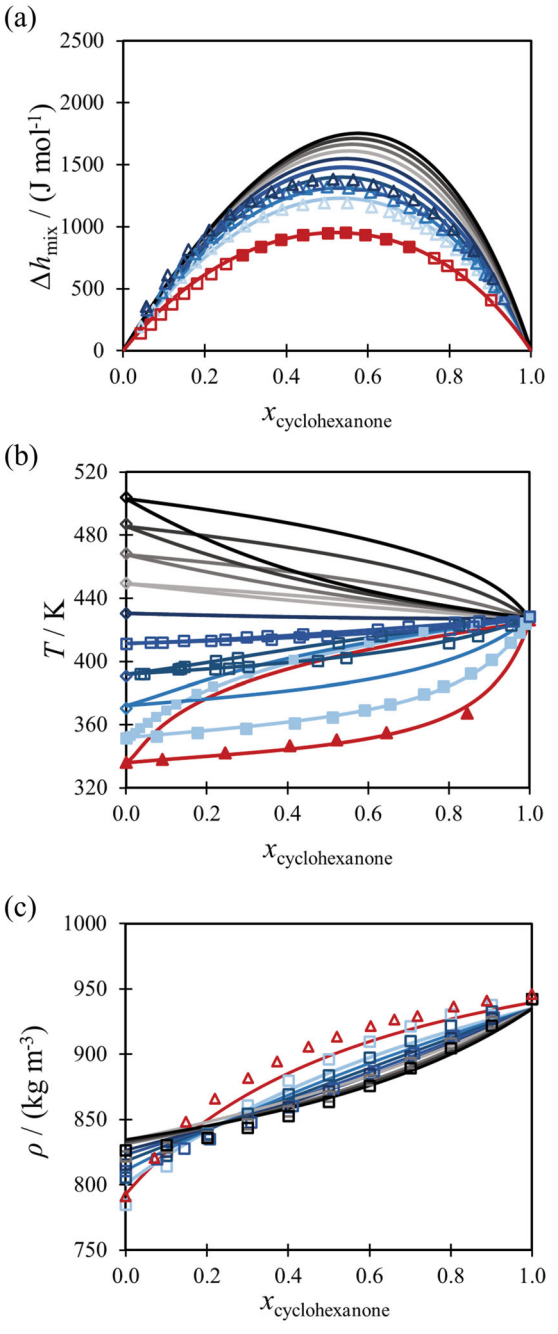

Figure 4. Selected thermodynamic properties of cyclohexanone with primary alcohols: methanol (red), ethanol to *n*-hexanol (light blue to dark blue), and *n*-heptanol to *n*-decanol (light grey to black). The continuous curves represent the SAFT-γ Mie calculations. The filled symbols [87, 89] represent the experimental data points included in the parameter estimation while the hollow symbols [87, 91–93, 109, 134] represent the data points used in the validation of the theoretical description. (a) Excess enthalpy at $T = 298.15$ K and $P = 101.3$ kPa. (b) Isobaric vapour–liquid equilibrium at $P = 94.80$ kPa for methanol and $P = 101.3$ kPa for ethanol to *n*-decanol. (c) Liquid density at $T = 293.15$ K and $P = 101.3$ kPa for methanol, and $T = 298.15$ K and $P = 101.3$ kPa for ethanol to *n*-decanol. The experimental data references corresponding to each mixture and its property are given in Table 7.

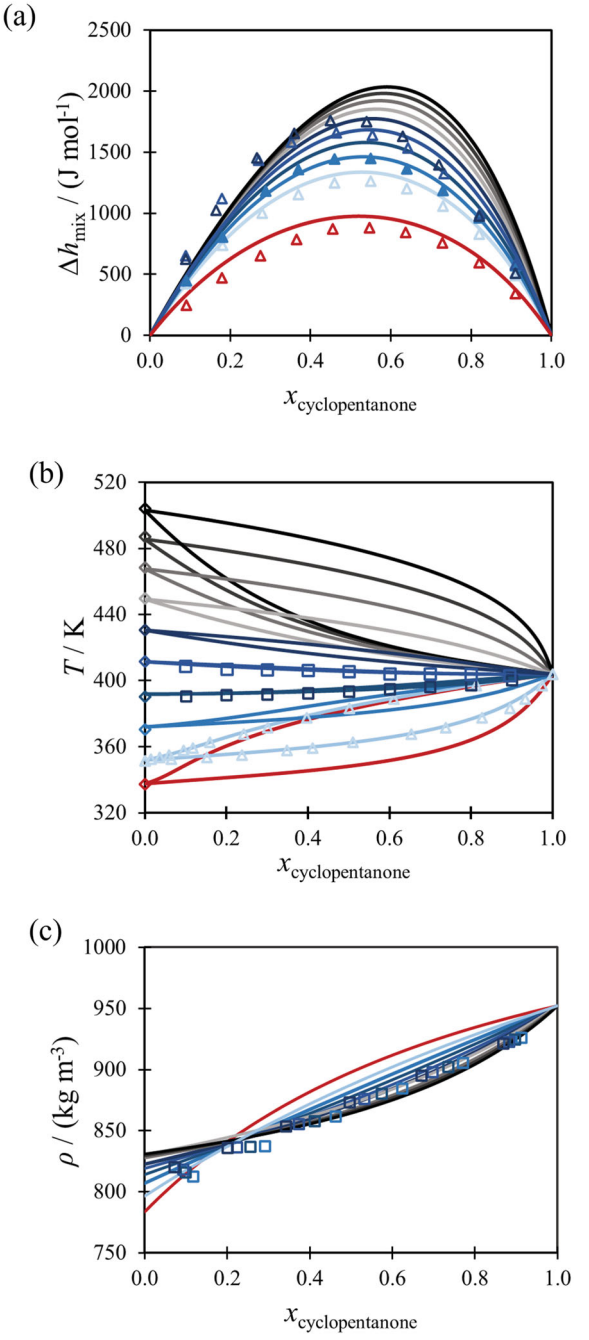

Figure 5. Selected thermodynamic calculations for binary mixtures of cyclopentanone with primary alcohols: methanol (red), ethanol to *n*-hexanol (light blue to dark blue), and *n*-heptanol to *n*-decanol (light grey to black). The continuous curves represent the SAFT-γ Mie calculations. The filled symbols [95] represent the experimental data points included in the parameter estimation while the hollow symbols [95–98, 134] represent the data points used in the validation of the theoretical description. (a) Excess enthalpy at T = 298.15 K and $P = 101.3$ kPa. (b) Isothermal vapour–liquid equilibrium at $P = 101.3$ kPa. (c) Liquid density at $T = 303.15$ K and P = 101.3 kPa. The experimental data references corresponding to each mixture and its property are given in Table 7.

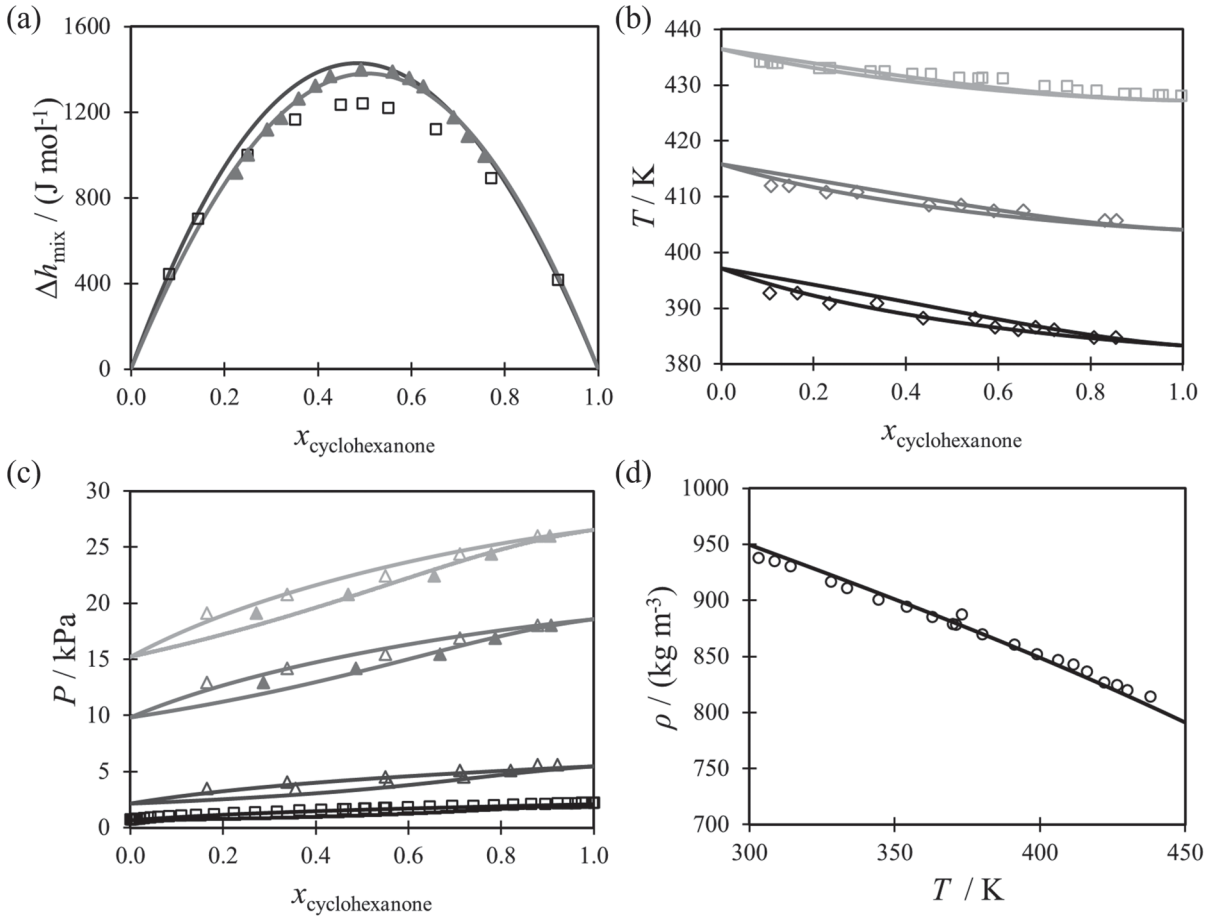

Figure 6. Selected thermodynamic properties of binary mixtures of cyclohexanone with cyclohexanol and with cyclopentanol. The continuous curves represent the SAFT-γ Mie calculations. The filled symbols [99, 104] represent the experimental data points included in the parameter estimation while the hollow symbols [100–104, 106] represent the data points used in the validation of the theoretical description. (a) Excess enthalpy at $T = 303.15$ K and P = 101.3 kPa for cyclohexanone + cyclohexanol [99] (medium grey) and at T = 298.15 K and $P = 101.3$ kPa for cyclohexanone + cyclopentanol [100] (black). (b) Isobaric vapour–liquid equilibrium at $P = 26.67$ kPa [101] (black), 52.66 kPa [101] (dark grey) and 100.8 kPa [102] (light grey) for cyclohexanone + cyclohexanol. (c) Isothermal vapour–liquid equilibrium at $T = 323.15$ K [103] (black), 343.15 K [105] (dark grey), 373.15 K [105] (grey), and 383.15 K [105] (light grey) for cyclohexanone + cyclohexanol. (d) Temperature–liquid density diagram at $x_{cyclohexanone} = 0.63$ and $P = 101.3$ kPa for cyclohexanone + cyclohexanol [106].

Figures 7(c), (d), and (e), it can be seen that the LLE region increases in size as the ring size of the cyclic ketone present in the mixture increases, reflecting the increased hydrophobicity of cyclic ketones.

Overall, excellent agreement is obtained between the experimental data and the SAFT-γ Mie calculations for mixtures of cyclic ketones with water as demonstrated by the low %AAD values in Table 7. The AAD value is 0.130 kJ mol^{-1} for the liquid excess enthalpy of cyclohexanone + water. The %AAD values are within 5.575% for the isothermal VLE for cyclohexanone + water and 7.649% for the isobaric VLLE for binary mixtures of cyclic ketones with water. The AAD values in composition are 0.023 mol.mol^{-1} for the isobaric LLE of cyclic ketones with water mixtures and 0.020 mol.mol^{-1} for the isobaric SLLE for cyclopentanone + water.

4. Menthone and 3-methylcyclohexanone, and their binary mixtures: predictions

Thermodynamic-property data are available for pure menthone and 3-methylcyclohexanone, and for binary mixtures of menthone with water, 1-decane, and menthol. In particular, data for the vapour pressure [73, 134, 155–161], saturated-liquid density [134, 162, 163], heat capacity, [164] and enthalpy of vaporisation [165] are available for both the pure compounds. Isobaric LLE data [55] for menthone + water at $P = 101.3$ kPa, isobaric VLE data [157] at $P = 23.99$ kPa, and isobaric SLE data [166] at $P = 101.3$ kPa for menthone + menthone are also available; these are used to assess the transferability of the interactions developed.

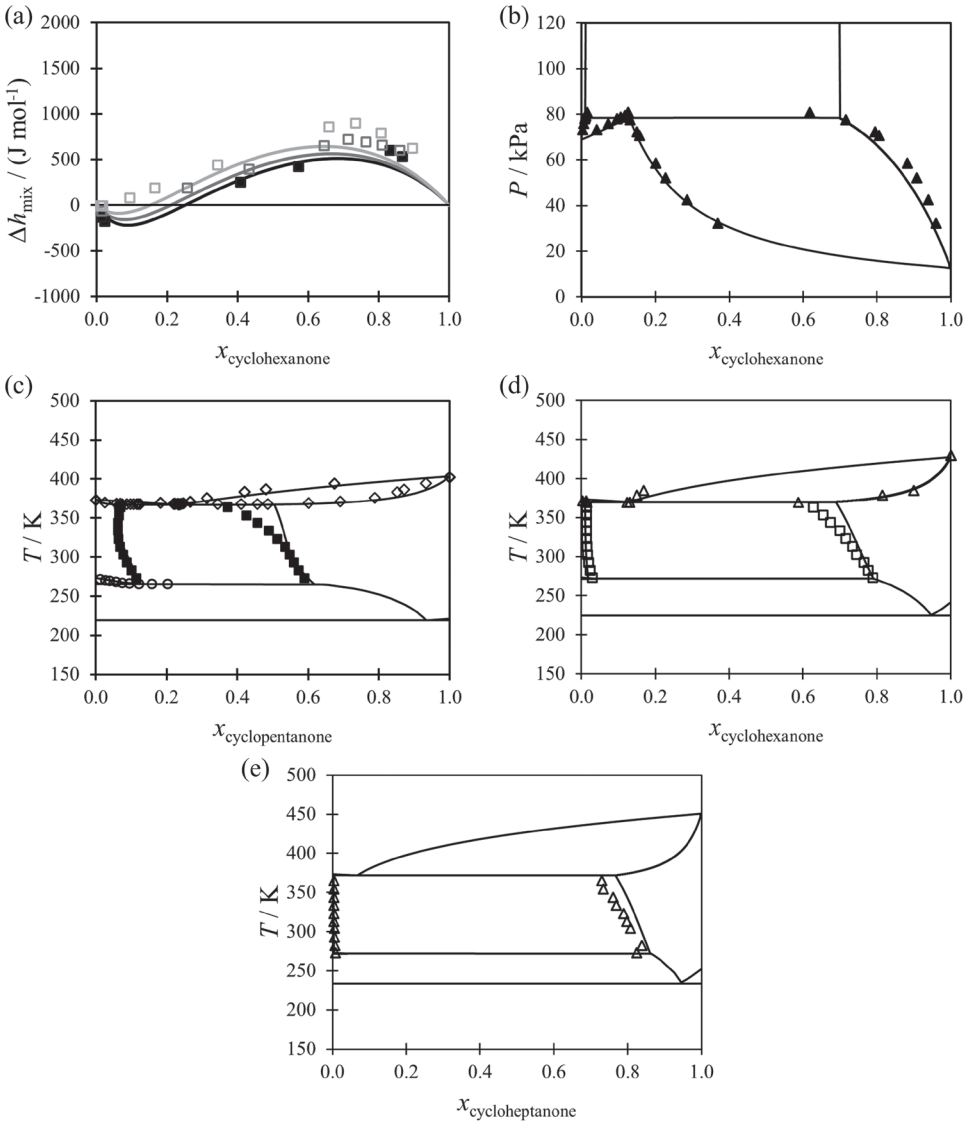

Figure 7. Selected thermodynamic properties of binary mixtures of cyclic ketones with water. The continuous curves represent the SAFT-γ Mie calculations. The filled symbols represent the experimental data points included in the parameter estimation while the hollow symbols represent the data points used in the validation of the theoretical description. (a) Excess enthalpy of cyclohexanone + water [130] at $T = 293.15$ K (black), 308.15 K (dark grey), and 323.15 K (light grey) and $P = 101.3$ kPa. (b) Isothermal phase diagram of cyclohexanone + water at $T = 363.15$ K with experimental data [104] for azeotropic vapour–liquid equilibrium. Isobaric phase diagrams of (c) cyclopentanone + water, (d) cyclohexanone + water, (e) cycloheptanone + water at atmospheric pressure, with experimental data for vapour–liquid [104, 132], liquid–liquid [131], and solid–liquid equilibria [133].

Each of the group interactions needed to model the mixtures of interest in this section have either been presented in previous work, or have been developed in the previous sections (cf. Figure 3). Therefore, all the calculations presented in this section for pure menthone, pure 3-methylcyclohexanone, and binary mixtures incorporating menthone, are fully predictive. This is also a test of the transferability of the unlike interactions in terms of their suitability to model the properties of pure menthone (i.e. we note that no experimental data of pure menthone has been used to determine any of the group interactions relevant for this compound). Vapour pressures, heat capacities, and enthalpies of vaporisation for menthone and 3-methylcyclohexanone are presented in Figure 8; a comparison of experimental values and SAFT-γ Mie predictions is provided. As can be seen in the figure, the properties of 3-methylcyclohexanone are predicted in very good agreement with experiment with %AAD values of 2.287% for the critical pressure, 5.676% for the vapour pressure, 4.266% for the saturated-liquid density, 2.537% for the saturated-heat capacity, and 8.728% for the enthalpy of vaporisation. In terms of menthone, larger deviations can be seen in the figure and the %AAD values are 9.124% for the critical temperature,

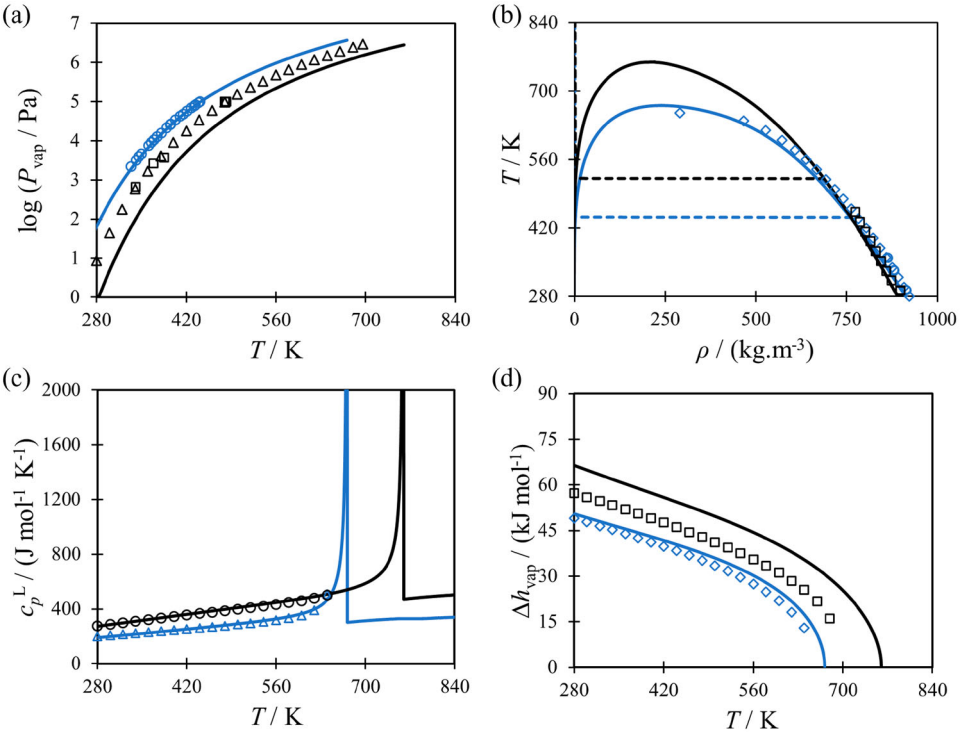

Figure 8. Selected thermodynamicproperties of pure 3-methylcyclohexanone (blue) and menthone (black). The continuous curves correspond to SAFT-γ Mie predictions and the hollow symbols to experimental data points. (a) Vapour pressure with experimental data of menthone [134, 155–161] and 3-methylcyclohexanone [73]. (b) Temperature–density diagram of menthone [162] and 3-methylcyclohexanone [134, 163], saturation densities are represented with continuous curves and isobaric density calculations at 101.3 kPa with dashed curves. (c) Saturated-liquid heat capacity with experimental data from ref. [164]. (d) Enthalpy of vaporisation with experimental data from ref. [165].

65.96% for the vapour pressure, 1.556% for the saturated-liquid density, 1.783% for the saturated-heat capacity, and 25.67% for enthalpy of vaporisation. High deviations are noted for critical temperature, vapour pressure, and the enthalpy of vaporisation of pure menthone, particularly at lower temperatures, although we note that uncertainties of 33.54% for the enthalpy of vaporisation, 9.864% for the vapour pressure and 2.442% for the critical temperature, are reported in the experimental source (NIST).

SAFT-γ Mie predictions for binary mixtures including menthone are presented in Figure 9. An extremely narrow region of azeotropic isobaric VLE is obtained both experimentally and theoretically for menthone + menthol at $P = 23.99$ kPa. The deviation between the calculated curve and the experimental data is a result of deviations in the vapour pressure of the pure compounds. This means that the predictions for this VLE curve cannot be improved with the current set of optimised parameters. However, as seen in Figure 9(b), the isobaric solid–liquid phase behaviour at $P = 101.3$ kPa of menthone + menthol including the location of the eutectic point are predicted in good agreement with experiment. The experimental eutectic point is found at $T^{exp.} = 261.2$ K and the predicted one is at $T^{calc.} = 257.1$ K. Close-to-ideal behaviour is observed for both the solubility of menthone in menthol, and *vice versa*. It is reassuring to predict this behaviour after developing the interaction parameters for the SAFT-γ Mie model using the experimental data for other smaller compounds. We also study the phase behaviour of menthone + water, as experimental data are available, and the parameters required to model this system have been developed without using these experimental data (cf. Section 3.4). A large region of isobaric LLE is predicted for menthone + water at $P = 101.3$ kPa, which is bounded by the VLLE curve at $T^{calc.} = 373.4$ K.

The quantitative agreement between the experimental data and theoretical calculations is excellent for these mixtures, as shown in Table 7. The %AAD value is 7.660% for the isobaric VLE and the AAD value is 0.038 mol.mol^{-1} for the isobaric SLE composition of menthone + menthol. The AAD value is 9.1×10^{-6} mol.mol^{-1} for the isobaric LLE composition of menthone + water.

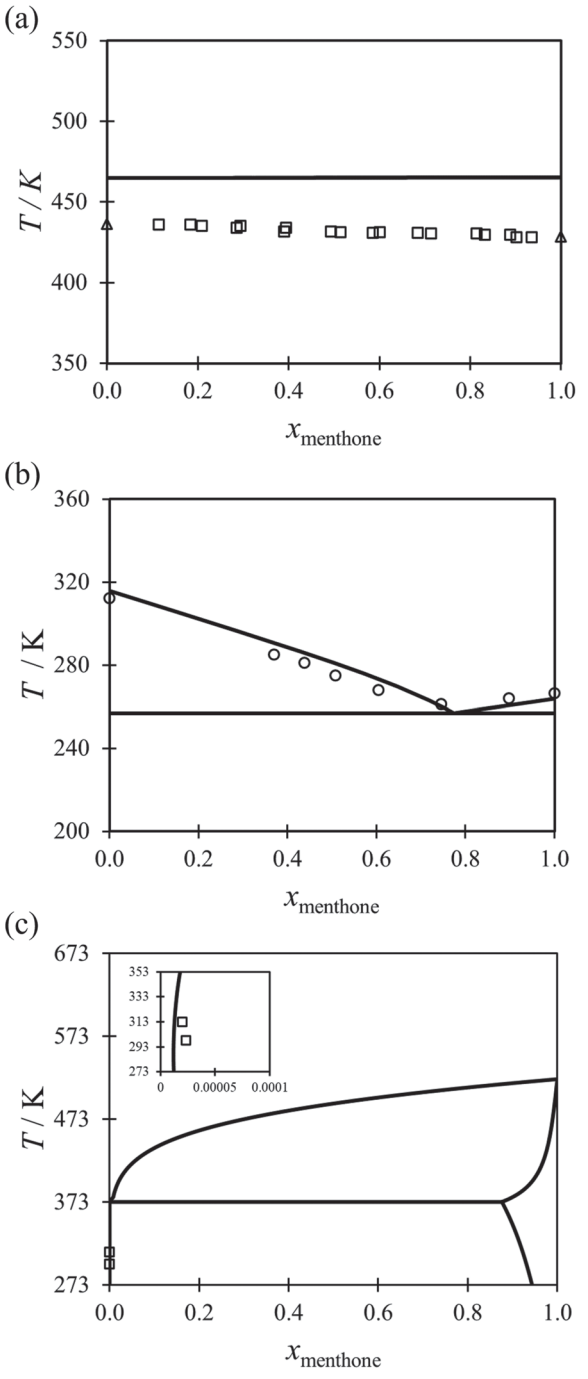

Figure 9. Selected thermodynamic properties of menthone + menthol and menthone + water mixtures. The symbols correspond to experimental data, while the continous curves correspond to SAFT-γ Mie predictions. (a) Isobaric vapour–liquid equilibria calculations at $P = 23.99$ kPa with experimental data from ref. [134, 157]. (b) Isobaric solid–liquid solubility at $P = 101.3$ kPa with experimental data from ref. [166]. (c) Isobaric liquid–liquid equilibria at $P = 101.3$ kPa data from ref. [55].

5. Overall agreement and AAD

The AAD and %AAD of the calculations compared to the relevant experimental data are provided in Table 7 to assess the quantitative accuracy of the SAFT-γ Mie model developed for the new cyclic ketone group. For pure compounds, deviations for the critical temperature, vapour pressure, saturated and isobaric liquid densities, heat capacity, and enthalpy of vaporisation are calculated. Bubble and dew temperatures, bubble and dew pressures, LLE and SLE composition, liquid density, and excess enthalpy are calculated for the binary mixtures studied. For each pure compound or mixture, the number of points considered to estimate the parameters, and the number of points considered to test the accuracy of the model developed, are reported. Temperature, pressure, and mole fraction ranges that are used as the input for the calculations are also included in the table.

We also present the calculated AAD and %AAD values in the form of column charts in Figure 10. For the %AAD values, the order of magnitude depends on the properties (highest for the excess enthalpy). For all the properties considered, the %AAD values are similar but slightly higher for the data points not considered in refining the interaction parameters. Overall for all the compounds considered in our work, the AAD values for the data points used for validation are 22.41 K for the critical temperature, 3.142 K for the bubble temperature, 3.922 K for the dew temperature, 48.38 kPa for the vapour pressure, 2.341 kPa for the bubble pressure, 1.304 kPa for the dew the pressure, 28.59 kg m^{-3} for the pure-fluid density, 7.556 kg m^{-3} for the mixture density, 2.924 kJ mol^{-1} for the enthalpy of vaporisation, 0.136 kJ mol^{-1} for the excess enthalpy, 0.099 for the SLE composition, 0.011 for the LLE composition, and 2.925 kJ mol^{-1} K^{-1} for the liquid heat capacity.

6. Conclusions

We have extended the application of the SAFT-γ Mie group-contribution approach by developing the new cyclic-ketone (cCO) group. Along with the new cCO–cCO interaction, 16 unlike group interactions have been characterised. To estimate parameters and assess the predictive accuracy of the model, we have examined numerous systems, including seven pure fluids (cyclobutanone, cyclopentanone, cyclohexanone, cycloheptanone, cyclooctanone, 3-methylcyclohexanone, and menthone), and 68 binary mixtures, selected according to the availability of experimental data. These mixtures

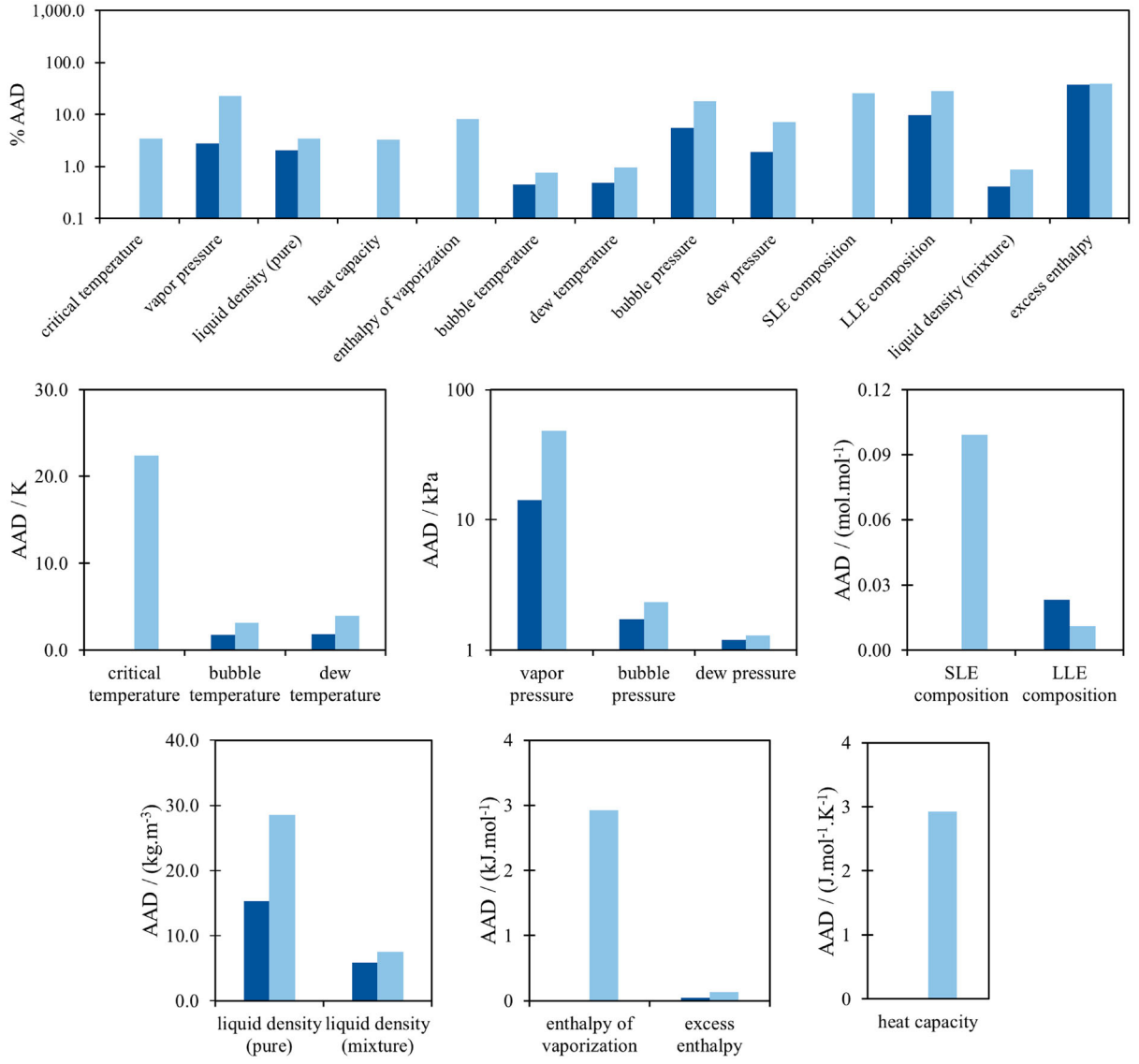

Figure 10. Overall %AAD and AAD for the properties considered in the current work. The results relating to the data used in the parameter estimation are presented in dark blue and the results relating to the predictions are in pale blue.

cover a wide range of solvent families, such as linear, branched, and cyclic alkanes, 1-alcohols, 2-alcohols, branched, and cyclic alcohols, secondary ketones, esters, aromatic compounds, and water. Among these, mixtures including cyclohexanone, cyclopentanone, or menthone have been studied in greater depth, as they represent small molecules comprising the new functional group characterised.

We have systematically assessed the transferability and quality of the new parameters characterised across varied mixtures and properties, including solid–liquid solubility, confirming the suitability of the model for the prediction of thermodynamic properties of larger molecules. Notably, we have successfully predicted the properties of mixtures containing menthone, achieving excellent agreement with the experimental data available. The newly introduced cCO functional group has also been applied to model other complex cyclic ketones enabling the prediction of thermodynamic properties and phase behaviour of new compounds and mixtures over a broad range of temperatures, pressures, and compositions. The current work paves the way for further applications in the pharmaceutical industry in systems including molecules such as testosterone and progesterone, as their molecular structures contain the cyclic ketone.

As discussed in the Introduction, a significant challenge in modelling fluids such as those that we have considered here is the structural complexity of their constituent molecules. The arrangement within these molecules of the different electron-withdrawing and electron-donating groups is expected to give rise, for example, to permanent molecular dipoles or quadrupoles,

leading in turn to intermolecular dipole–dipole, quadrupole–quadrupole, and dipole–quadrupole interactions. Some account of these interactions is implicitly taken through the incorporation of association within the model fluid. However, in adopting a group-contribution approach in the fashion described here, wherein explicit account is taken of interactions only at the level of the functional groups, one cannot provide a complete treatment of the impact of these intermolecular interactions on the properties of the fluid. For greater modelling accuracy, one can introduce second-order group effects. In the context of SAFT-γ Mie, we classify such effects according to whether or not, when one of the groups exists in a particular molecular environment, the unlike interaction (characterising how two unlike groups interact with each other) differs from the regular unlike interaction. Such second-order group effects have been discussed in Ref. [14], including examples adopted within the SAFT-γ Mie approach. The underlying philosophy of the approach, however, is to avoid unnecessary use of second-order group interactions. The high-quality descriptions and predictions of the thermodynamic properties of the fluids considered here provide a testament to the power of the method at the level of the first-order groups.

Disclosure statement

No potential conflict of interest was reported by the author(s).

Funding

We gratefully acknowledge support from Eli Lilly and Company through the PharmaSEL Programme and joint EPSRC/Lilly Prosperity Partnership (EP/T005556/1). We also acknowledge financial support from the Engineering and Physical Sciences Research Council (EPSRC) of the UK (grants GR/T17595, GR/N35991, EP/E016340, EP/P006965, and EP/J014958/1) to the Molecular Systems Engineering group. Amparo Galindo is thankful to the Royal Academy of Engineering and Eli Lilly and Company for support of a Research Chair (Grant RCSRF18193). We wish to acknowledge the use of the EPSRC funded Physical Sciences Data-science Service hosted by the University of Southampton and STFC under grant number EP/S020357/1.

Data statement

Data underlying this article can be accessed on Zenodo at https://doi.org/10.5281/zenodo.15211295 and used under the Creative Commons Attribution license.

References

[1] A. Fredenslund, R.L. Jones and J.M. Prausnitz, AIChE J. **21**, 1086–1099 (1975). doi:10.1002/aic.v21:6.

[2] T. Holderbaum and J. Gmehling, Fluid. Phase. Equilib. **70**, 251–265 (1991). doi:10.1016/0378-3812(91)85038-V.

[3] S.-T. Lin and S.I. Sandler, Ind. Eng. Chem. Res. **41**, 899–913 (2002). doi:10.1021/ie001047w.

[4] V. Papaioannou, T. Lafitte, C. Avendaño, C.S. Adjiman, G. Jackson, E.A. Müller and A. Galindo, J. Chem. Phys. **140**, 054107 (2014). doi:10.1063/1.4851455.

[5] S. Dufal, V. Papaioannou, M. Sadeqzadeh, T. Pogiatzis, A. Chremos, C.S. Adjiman, G. Jackson and A. Galindo, J. Chem. Eng. Data **59**, 3272–3288 (2014). doi:10.1021/je500248h.

[6] S. Dufal, T. Lafitte, A.J. Haslam, A. Galindo, G.N. Clark, C. Vega and G. Jackson, Mol. Phys. **113**, 948–984 (2015). doi:10.1080/00268976.2015.1029027.

[7] S. Dufal, T. Lafitte, A.J. Haslam, A. Galindo, G.N.I. Clark, V. Vega and G. Jackson, Mol. Phys. **116**, 283–285 (2018). doi:10.1080/00268976.2017.1402604.

[8] W.G. Chapman, K.E. Gubbins, G. Jackson and M. Radosz, Fluid Phase Equilib. **52**, 31–38 (1989). doi:10.1016/0378-3812(89)80308-5.

[9] W.G. Chapman, K.E. Gubbins, G. Jackson and M. Radosz, Ind. Eng. Chem. Res. **29**, 1709–1721 (1990). doi:10.1021/ie00104a021.

[10] A. Gil-Villegas, A. Galindo, P.J. Whitehead, S.J. Mills, G. Jackson and A.N. Burgess, J. Chem. Phys.**106**, 4168–4186 (1997). doi:10.1063/1.473101.

[11] T. Lafitte, A. Apostolakou, C. Avendaño, A. Galindo, C.S. Adjiman, E.A. Müller and G. Jackson, J. Chem. Phys. **139**, 154504 (2013). doi:10.1063/1.4819786.

[12] M. Sadeqzadeh, V. Papaioannou, S. Dufal, C.S. Adjiman, G. Jackson and A. Galindo, Fluid. Phase. Equilib. **407**, 39–57 (2016). doi:10.1016/j.fluid.2015.07.047.

[13] P. Hutacharoen, S. Dufal, V. Papaioannou, R.M. Shanker, C.S. Adjiman, G. Jackson and A. Galindo, Ind. Eng. Chem. Res. **56**, 10856–10876 (2017). doi:10.1021/acs.iecr.7b00899.

[14] A.J. Haslam, A. González-Pérez, S. Di Lecce, S.H. Khalit, F.A. Perdomo, S. Kournopoulos, M. Kohns, T. Lindeboom, M. Wehbe, S. Febra, G. Jackson, C.S. Adjiman and A. Galindo, J. Chem. Eng. Data. **65**, 5862–5890 (2020). doi:10.1021/acs.jced.0c00746.

[15] S.A. Febra, T. Bernet, C. Mack, J. McGinty, I.I. Onyemelukwe, S.J. Urwin, J. Sefcik, C.S. Adjiman, G. Jackson and A. Galindo, Fluid. Phase. Equilib. **540**, 113002 (2021). doi:10.1016/j.fluid.2021.113002.

[16] M. Wehbe, A.J. Haslam, G. Jackson and A. Galindo, Fluid. Phase. Equilib. **560**, 113504 (2022). doi:10.1016/j.fluid.2022.113504.

[17] T. Bernet, M. Wehbe, S.A. Febra, A.J. Haslam, C.S. Adjiman, G. Jackson and A. Galindo, J. Chem. Eng. Data **69**, 650–678 (2024). doi:10.1021/acs.jced.3c00358.

[18] M. Valsecchi, A. Galindo and G. Jackson, Macromolecules **56**, 9952–9968 (2023). doi:10.1021/acs.macromol.3c01336.

[19] M. Valsecchi, A. Galindo and G. Jackson, Fluid. Phase. Equilib. **577**, 113952 (2024). doi:10.1016/j.fluid.2023.113952.

[20] A. Alyazidi, S. Paliwal, F.A. Perdomo, A. Mead, M. Guo, J.Y.Y. Heng, T. Bernet, A.J. Haslam, C.S. Adjiman, G. Jackson and A. Galindo, Ind. Eng. Chem. Res. **63**, 20397–20423 (2024). doi:10.1021/acs.iecr.4c02995.

[21] F.A. Perdomo, S.H. Khalit, C.S. Adjiman, A. Galindo and G. Jackson, AIChE J. **67**, e17194 (2021). doi:10.1002/aic.v67.3.

[22] F.A. Perdomo, S.H. Khalit, E.J. Graham, F. Tzirakis, A.I. Papadopoulos, I. Tsivintzelis, P. Seferlis, C.S. Adjiman, G. Jackson and A. Galindo, Fluid. Phase. Equilib. **566**, 113635 (2023). doi:10.1016/j.fluid.2022.113635.

[23] O.L. Watson, S. Jonuzaj, J. McGinty, J. Sefcik, A. Galindo, G. Jackson and C.S. Adjiman, Org. Process. Res. Dev. **25**, 1123–1142 (2021). doi:10.1021/acs.oprd.0c00516.

[24] D.H. Bowskill, U.E. Tropp, S. Gopinath, G. Jackson, A. Galindo and C.S. Adjiman, Mol. Syst. Des. Eng **5**, 493–510 (2020). doi:10.1039/C9ME00089E.

[25] Y.S. Lee, E. Graham, G. Jackson, A. Galindo and C.S. Adjiman, in *Computer Aided Chemical Engineering*, edited by A.A. Kiss, E. Zondervan, R. Lakerveld, L. Özkan (Elsevier, London, 2019), Vol. 46, pp. 37–42.

[26] Y.S. Lee, E.J. Graham, A. Galindo, G. Jackson and C.S. Adjiman, Comput. Chem. Eng. **136**, 106802 (2020). doi:10.1016/j.compchemeng.2020.106802.

[27] Y.S. Lee, A. Galindo, G. Jackson and C.S. Adjiman, in *Computer Aided Chemical Engineering*, edited by M. Türkay, R. Gani (Elsevier, London, 2021), Vol. 50, pp. 167–172.

[28] Y.S. Lee, G. Jackson, A. Galindo and C.S. Adjiman, in *Computer Aided Chemical Engineering*, edited by Y. Yamashita, M. Kano (Elsevier, London, 2022), Vol. 49, pp. 1225–1230.

[29] Y.S. Lee, G. Jackson, A. Galindo and C.S. Adjiman, Chem. Eng. Res. Des. **200**, 615–636 (2023). doi:10.1016/j.cherd.2023.11.007.

[30] Y.S. Lee, A. Galindo, G. Jackson and C.S. Adjiman, Comput. Chem. Eng. **174**, 108204 (2023). doi:10.1016/j.compchemeng.2023.108204.

[31] R. Rios-Estepa, G.W. Turner, J.M. Lee, R.B. Croteau and B.M. Lange, Proc. Nat. Acad. Sci. **105**, 2818–2823 (2008). doi:10.1073/pnas.0712314105.

[32] S.M. Vilas-Boas, I.W. Cordova, D.O. Abranches, J.A.P. Coutinho, O. Ferreira and S.P. Pinho, Ind. Eng. Chem. Res. **62**, 5326–5335 (2023). doi:10.1021/acs.iecr.2c03991.

[33] H. Cho, K. Sowndhararajan, J.-W. Jung, J.-W. Jhoo and S. Kim, J. Life. Sci.**23**, 933–940 (2013). doi:10.5352/JLS.2013.23.7.933.

[34] U. Ravid, E. Putievsky and I. Katzir, Flavour. Fragr. J. **9**, 139–142 (1994). doi:10.1002/ffj.v9:3.

[35] E. Frérot, A. Bagnoud and C. Vuilleumier, Flavour. Fragr. J. **17**, 218–226 (2002). doi:10.1002/ffj.v17:3.

[36] M. Butnariu, *Bioprospecting of Plant Biodiversity for Industrial Molecules* (John Wiley & Sons, Ltd., 2021), Chapter 13, pp. 261–292.

[37] N. Hudz, L. Kobylinska, K. Pokajewicz, V. Horčinová Sedláčková, R. Fedin, M. Voloshyn, I. Myskiv, J. Brindza, P.P. Wieczorek and J. Lipok, Molecules **28**, 7444 (2023). doi:10.3390/molecules28217444.

[38] A. Kapp, M. Roasto, A. Raal, T. Püssa, H. Vuorela, P. Tammela and P. Vuorela, Planta. Med. **86**, 1089–1096 (2020). doi:10.1055/a-1158-1699.

[39] J.M. Davidson, R.S.T. Linforth, T.A. Hollowood and A.J. Taylor, J. Agric. Food. Chem. **47**, 4336–4340 (1999). doi:10.1021/jf9901082.

[40] D.Y.-H. Yeung, T. Lee, G. Grant, M. Ma and E. Kwong, J. Pharm. Biomed. Anal. **30**, 1469–1477 (2003). doi:10.1016/S0731-7085(02)00484-3.

[41] I. Ovejero-López, A.-M. Haahr and W.L.P. Bredie, J. Agric. Food. Chem. **52**, 8119–8126 (2004). doi:10.1021/jf048716r.

[42] A. Kiełtyka-Dadasiewicz and A. Kubat-Sikorska, Arch. Physiother. Glob. Res. **22**, 53–57 (2018). doi:10.15442/apgr.

[43] N.R. Desam, A.J. Al-Rajab, M. Sharma, M.M. Mylabathula, R.R. Gowkanapalli and M. Albratty, J. King Saud Univ. Sci. **31**, 528–533 (2019). doi:10.1016/j.jksus.2017.07.013.

[44] H. Oumzil, S. Ghoulami, M. Rhajaoui, A. Ilidrissi, S. Fkih-Tetouani, M. Faid and A. Benjouad, Phytother. Res. **16**, 727–731 (2002). doi:10.1002/ptr.v16:8.

[45] M.G. Zaia, T. d. O. Cagnazzo, K.A. Feitosa, E.G. Soares, L.H. Faccioli, S.M. Allegretti, A. Afonso and F. d. F. Anibal, Front. Pharmacol. **7** (2016), Article 170. doi:10.3389/fphar.2016.00170.

[46] Y.-H. Su and J.-Y. Lin, Int. J. Mol. Sci. **23**, 4011 (2022).

[47] J. Xue, H. Li, X. Deng, Z. Ma, Q. Fu and S. Ma, Pharmacol. Biochem. Behav. **134**, 42–48 (2015). doi:10.1016/j.pbb.2015.04.014.

[48] L.R. Lizarraga-Valderrama, Phytother. Res. **35**, 657–679 (2021). doi:10.1002/ptr.v35.2.

[49] O. Ahrens, W. Johanns, U. Kölling, J. Janssen and L. Greiner, Med. Klin. **99**, 279–284 (2004). doi:10.1007/s00063-004-1041-6.

[50] H. Renon, *Fluid Phase Equilibria* (Elsevier Science Publishers B.V., 1985), Vol. 24, pp. 87–114.

[51] D.S. Abrams and J.M. Prausnitz, AIChE J. **21**, 116–128 (1975). doi:10.1002/aic.v21:1.

[52] G.M. Wilson, J. Am. Chem. Soc. **86**, 127–130 (1964). doi:10.1021/ja01056a002.

[53] A. Klamt, in *COSMO-RS*, edited by A. Klamt (Elsevier: Amsterdam, 2005), pp. 83–107.

[54] I. Batiu, Fluid. Phase. Equilib. **198**, 111–121 (2002). doi:10.1016/S0378-3812(01)00759-2.

[55] S.M. Vilas-Boas, M.C. da Costa, J.A.P. Coutinho, O. Ferreira and S.P. Pinho, Ind. Eng. Chem. Res. **61**, 3154–3167 (2022). doi:10.1021/acs.iecr.1c04196.

[56] M.H. Abraham, Chem. Soc. Rev **22**, 73–83 (1993). doi:10.1039/cs9932200073.

[57] M.H. Abraham, A. Ibrahim and A.M. Zissimos, J. Chromatogr. A **1037**, 29–47 (2004). doi:10.1016/j.chroma.2003.12.004.

[58] A.A. Petrauskas and E.A. Kolovanov, Perspect. Drug Discov. Des. **19**, 99–116 (2000). doi:10.1023/A:1008719622770.

[59] G. Mie, Ann. Phys. **316**, 657–697 (1903). doi:10.1002/andp.v316:8.

[60] K. Betts, J. Rowlinson and G. Saville, *AIChE Journal* (John Wiley & Sons, Ltd, 1977), Vol. 23, p. 213.

[61] F.A. Perdomo, G. Jackson, A. Galindo and C.S. Adjiman, In *Computer Aided Chemical Engineering*, edited by A.C. Kokossis, M.C. Georgiadis, E. Pistikopoulos (Elsevier, London, 2023), Vol. 52, pp. 973–978.

[62] F.E. Pereira, G. Jackson, A. Galindo and C.S. Adjiman, Comput. Chem. Eng. **36**, 99–118 (2012). doi:10.1016/j.compchemeng.2011.07.009.

[63] O. Shvaro, A. Peshchenko, A. Sachek, V. Vasil'ev and N. Smirnova, Deposited Doc. VINITI 1–15 **87** (1987).
[64] J. Gmehling, Pure compound data from DDB. **1983**, 1.
[65] A. Gonthier-Vassal and H. Szwarc, Thermochim. Acta. **320**, 141–154 (1998). doi:10.1016/S0040-6031(98)00409-2.
[66] Y.P. Handa, R.E. Hawkins and J.J. Murray, J. Chem. Thermodyn. **16**, 623–632 (1984). doi:10.1016/0021-9614(84)90042-9.
[67] V. Štejfa, M. Fulem and K. Ružička, J. Chem. Thermodyn. **144**, 106013 (2020). doi:10.1016/j.jct.2019.106013.
[68] J. Dykyi and M. Repas, Saturation Vapor Pressure of Organic Compounds. *Veda Vydavatelstvo Slovenskej Akademie Vied, Bratislava* **1979**.
[69] D. Hopfe, Thermophysical data of pure substances. *Data Compilation of FIZ CHEMIE Germany* **1990**, 1.
[70] gPROMS, https://www.siemens.com/global/en/products/automation/industry-software/gproms-digital-process-design-and-operations.html (accessed Jul. 16, 2024).
[71] C. Polo, S. Otin and C. Gutierrez Losa, J. Chem. Thermodyn. **14**, 309–312 (1982). doi:10.1016/0021-9614(82)90048-9.
[72] R. Vandoni, Meml. Poudres **28**, 236–251 (1938).
[73] A. Aucejo, M. Cruz Burguet, R. Munoz and M.I. Vazquez, J. Chem. Eng. Data **38**, 379–382 (1993). doi:10.1021/je00011a011.
[74] T. Roscher, FIZ Report 2051 (1970).
[75] M. Cruz Burguet, J.B. Monton, M. Sanchotello and M.I. Vazquez, J. Chem. Eng. Data **38**, 328–331 (1993). doi:10.1021/je00010a037.
[76] K. Tamura, S. Murakami and R. Fujishiro, J. Chem. Thermodyn. **13**, 47–52 (1981). doi:10.1016/S0021-9614(81)80007-9.
[77] D. Venkatesulu and M. Rao, Asian J. Chem. **4**, 452–456 (1992).
[78] X.N. Yang and J.H. Zhang, J. Chem. Thermodyn. **26**, 449–456 (1994). doi:10.1006/jcht.1994.1054.
[79] K.P.C. Rao and K.S. Reddy, Phys. Chem. Liq. **17**, 297–304 (1988). doi:10.1080/00319108808078565.
[80] K.C. Rao, K.S. Reddy and M. Ramakrishna, Fluid. Phase. Equilib. **41**, 303–316 (1988). doi:10.1016/0378-3812(88)80015-3.
[81] B.S. Mahl and H. Kaur, Thermochim. Acta. **112**, 351–364 (1987). doi:10.1016/0040-6031(87)88292-8.
[82] D. Wei, S. Han and B. Wang, J. Chem. Thermodyn. **76**, 87–92 (2014). doi:10.1016/j.jct.2014.03.007.
[83] T.E.V. Prasad, A.N. Raju, N. Sriram and D.H.L. Prasad, Fluid. Phase. Equilib.**227**, 37–39 (2005). doi:10.1016/j.fluid.2004.10.027.
[84] L. Koldobskaya, A. Gaile, L. Semenov, E. Zhmaev, S. Kuznetsova and N. Rumyantseva, *Deposited Doc. VINITI* **1987**, 1–17.
[85] B. Marongiu, S. Dernini and A.M. Polcaro, J. Chem. Eng. Data **31**, 185–189 (1986). doi:10.1021/je00044a017.
[86] A. Krishnaiah, K.N. Surendranath and M. Ramakrishna, Proc. Indian Acad. Sci. Chem. Sci. **100**, 323–328 (1988). doi:10.1007/BF02840542.
[87] J.P. Chao and M. Dai, J. Chem. Thermodyn. **21**, 977–983 (1989). doi:10.1016/0021-9614(89)90157-2.
[88] K. Zhang, D. Xu, Y. Zhou, P. Shi, J. Gao and Y. Wang, J. Chem. Eng. Data **63**, 2038–2045 (2018). doi:10.1021/acs.jced.8b00033.
[89] T.E.V. Prasad, B.V. Sudheendra, G. Veerendra, K. Venugopalachary, A.V. Sarma and D.H.L. Prasad, Phys. Chem. Liq. **45**, 525–530 (2007). doi:10.1080/00319100701311445.
[90] I. Marchenko, M. Vasil'eva, L. Komarova and Y. Garber, Zh. Prikl. Khim. **58**, 2069–2073 (1985).
[91] G. Mihaila, V. Ababi, P. Onu and C. Luca, Rev. Chim. Bucharest. **30**, 533–535 (1979).
[92] V. Granzhan and O. Kirillova, Zh. Prikl. Khim. **45**, 239–240 (1972).
[93] A.G. Gilani and S. Ramezani, J. Chem. Eng. Data **63**, 4703–4719 (2018).
[94] A.G. Gilani and A. Mirkhalili, J. Chem. Eng. Data **66**, 3934–3950 (2021). doi:10.1021/acs.jced.1c00545.
[95] H. Iloukhani and M. Fattahi, J. Mol. Liq. **171**, 37–42 (2012). doi:10.1016/j.molliq.2012.04.003.
[96] O. Rakhmetova, A. Taghipour, G. Will, R.J. Brown and T.J. Rainey, J. Chem. Eng. Data **68**, 366–374 (2023). doi:10.1021/acs.jced.2c00624.
[97] E. Katunina, I. Marchenko, O. Chervova, L. Polyakova and Y. Garber, Zh. Prikl. Khim **65**, 2028–2033 (1992).
[98] M.V. Prabhakara Rao and P.R. Naidu, J. Chem. Thermodyn. **8**, 73–76 (1976). doi:10.1016/0021-9614(76)90153-1.
[99] C. Huiting and W. Fuhua, *Huaxue Gongcheng Xi'an* (Xi'an (Shaanxi): Editorial Department of Chemical Engineering, 1984), Vol. 12, pp. 44–47.
[100] P. Ma, S. Xia and X. Wu, Wuli Huaxue Xuebao **18**, 644–648 (2002).
[101] S.R. Goodwin and D.M.T. Newsham, J. Chem. Eng. Data **19**, 363–366 (1974). doi:10.1021/je60063a026.
[102] Y. Zeng, Y. Yang, H. Luo, Z. Duan and W. Liu, Huaxue Gongcheng Xi'an **35**, 33–36 (2007).
[103] R. Abbas and J. Gmehling, Fluid. Phase. Equilib. **267**, 119–126 (2008). doi:10.1016/j.fluid.2008.02.021.
[104] I. Gorodetskii, A. Morachevskii and V. Olevskii, Vestn. Leningr. Univ. Ser. 4 Fiz. Khim. **4**, 136–139 (1959).
[105] I. Gorodetskii and V. Olevskii, Tr. Gos. Nauchno Issled. Proektn. Inst. Azotn. Promst. Prod. Org. Sin **10**, 99–112 (1959).
[106] I. Golubev and M. Frolova, Tr. Gos. Nauchno Issled. Proektn. Inst. Azotn. Promst. Prod. Org. Sin**10**, 38–44 (1959).
[107] V.K. Sharma, J. Kataria and S. Bhagour, J. Mol. Liq. **195**, 132–138 (2014). doi:10.1016/j.molliq.2014.02.009.
[108] K. Tamura, J. Chem. Thermodyn. **33**, 1345–1353 (2001). doi:10.1006/jcht.2001.0851.
[109] I. Marchenko, O. Oleneva, L. Polyakova, I. Mis'ko and Y. Garber, J. Appl. Chem. USSR **62**, 2559–2563 (1989).
[110] V. Ponomarev, A. Lebedev and V. Timofeev, Tr. Mosk. Inst. Tonkoi Khim. Tekhnol **9**, 240–246 (1979).
[111] A. Van de Vloed, Bull. Soc. Chim. Belg **48**, 229–268 (1939). doi:10.1002/bscb.v48.7.
[112] M.M.L. Labruyère-Verhavert, Bull. Soc. Chim. Belges **60**, 270–281 (1951). doi:10.1002/bscb.v60:5/6.
[113] Q. Shang, J. Xiao, X. Liu, Y. Ling, W. Liu, G. Cui, X. Shi, S. Xia and B. Tang, J. Chem. Thermodyn. **164**, 106622 (2022). doi:10.1016/j.jct.2021.106622.

[114] J. Rubio, A. Moreau, J.J. Segovia, M.A. Villamañán and M.C. Martín, J. Mol. Liq. **303**, 112404 (2020). doi:10.1016/j.molliq.2019.112404.
[115] C. Younts, Ph.D. thesis, University Of Washington, 1972.
[116] K. Tamura and T. Yamasawa, J. Therm. Anal. Calorim.**69**, 849–863 (2002). doi:10.1023/A:1020655906079.
[117] L. Kudryavtseva, M. Kuus, H. Kirss and E. Siimer, ELDATA Int. Electron. J. Phys. Chem. Data **5**, 65–77 (1999).
[118] G. Weissenberger, F. Schuster and R. Henke, Monatsh. Chem. Verwandte Teile Anderer Wissenschaften **46**, 47–56 (1925). doi:10.1007/BF01525489.
[119] L. Bernazzani, V. Mollica and M.R. Tiné, Fluid. Phase. Equilib. **203**, 15–29 (2002). doi:10.1016/S0378-3812(02)00169-3.
[120] P.P. Divakar, B.V. Rao and K. Samatha, E-J. Chem. **9**, 681241 (2012).
[121] L. Zhou, Y. Wang, Y. Zhang, J. Shi, G.C. Benson and B.C.-Y. Lu, Thermochim. Acta. **189**, 57–63 (1991). doi:10.1016/0040-6031(91)87099-I.
[122] J. Gao, K. Zhang, D. Xu, L. Zhang, N. Chen and C. Li, J. Chem. Eng. Data **62**, 1948–1954 (2017). doi:10.1021/acs.jced.6b00877.
[123] F. Kohler, E. Liebermann, R. Schano, H.E. Affsprung, J.K. Morrow, K. Sosnkowska-Kehiaian and H. Kehiaian, J. Chem. Thermodyn. **7**, 241–250 (1975). doi:10.1016/0021-9614(75)90061-0.
[124] K. Seshadri, N.P. Rao and K.C. Reddy, Z. Phys. Chem. Neue Fol. **89**, 108–121 (1974).
[125] G.J. Pierotti, C.H. Deal and E.L. Derr, Ind. Eng. Chem. **51**, 95–102 (1959). doi:10.1021/ie50589a048.
[126] R. Murogova, G. Tudorovskaya, I. Gridin, A. Yurchuk, N. Pleskach, V. Kozlova, T. Bazyleva, N. Safonova and L. Serafimov, J. Appl. Chem. USSR **45**, 837–841 (1972).
[127] S. Stoeck and K. Moerke, Leuna-Protokoll 3141 (1991).
[128] T. Roscher, FIZ Report 12091 (1965).
[129] A. Aarna and T. Kaps, Eesti NSV Tead. Akad. Toim. Keem. Geol **23**, 16–21 (1974).
[130] V. Belousov and E. Sokolova, Vestn. Leningr. Univ. Ser. 4 Fiz. Khim **16**, 90–93 (1966).
[131] R.M. Stephenson, J. Chem. Eng. Data **37**, 80–95 (1992). doi:10.1021/je00005a024.
[132] G. Albanesi, I. Pasquon and P. Genoni, Chim. Ind. Milan **39**, 814–821 (1957).
[133] V. Bertini and P. Pino, Chim. Ind. Milan **41**, 195–201 (1959).
[134] NIST Chemsitry WebBook: https://webbook.nist.gov/. (accessed Jul. 17, 2024).
[135] T. Bernet, S. Paliwal, A. Alyazidi, R. Standish, A.J. Haslam, C.S. Adjiman, G. Jackson and A. Galindo, Mol. Phys. **122** (21–22), e2394132 (2024).
[136] P. Hutacharoen, Ph.D. thesis, Imperial College London, London, 2017.
[137] T. Lindeboom, Ph.D. thesis, Imperial College London, London, 2019.
[138] S.W. Benson and G.B. Kistiakowsky, J. Am. Chem. Soc.**64**, 80–86 (1942). doi:10.1021/ja01253a021.
[139] F. Glaser and H. Rüland, Chem. Ing. Tech. **29**, 772–775 (1957). doi:10.1002/cite.v29:12.
[140] V. Markovnik, O. Shvaro, A. Sachek and A. Peshchenko, Izv. Vyssh. Uchebn. Zaved. Khim. Khim. Tekhnol. **26**, 698–702 (1983).
[141] E.F. Meyer and C.A. Hotz, J. Chem. Eng. Data **21**, 274–279 (1976). doi:10.1021/je60070a035.
[142] M. Teodorescu, A. Barhala and D. Dragoescu, J. Chem. Thermodyn. **38**, 1432–1437 (2006). doi:10.1016/j.jct.2006.01.010.
[143] V. Durov, N. Lifanova and A. Artykov, Zh. Fiz. Khim **60**, 2740–2744 (1986).
[144] G. Liessmann, W. Schmidt and S. Reiffarth, Recommended Thermophysical Data. **1995**, 1.
[145] E. Kuss, Z. Angew. Phys. **7**, 372–378 (1955).
[146] T. Tyvina, V. Fokina and A. Poljakov, Zh. Prikl. Khim. **58**, 442–445 (1985).
[147] N. Nakamura, H. Suga and S. Seki, Bull. Chem. Soc. Jpn.**53**, 2755–2761 (1980). doi:10.1246/bcsj.53.2755.
[148] V.K. Sharma, S. Malik and S. Solanki, J. Chem. Eng. Data **62**, 623–632 (2017). doi:10.1021/acs.jced.6b00606.
[149] J.S. Chickos, S. Hosseini and D.G. Hesse, Thermochim. Acta. **249**, 41–62 (1995). doi:10.1016/0040-6031(95)90670-3.
[150] K. Nishikawa, K. Tamura and S. Murakami, J. Chem. Thermodyn. **30**, 229–240 (1998). doi:10.1006/jcht.1997.0296.
[151] X. Wang, H. Wang, B. Yan and D. Jiang, Zhengzhou Daxue Xuebao Gongxue Ban **33**, 48–50 (2012).
[152] T. Boublik and B.C.Y. Lu, J. Chem. Eng. Data **22**, 331–333 (1977). doi:10.1021/je60074a027.
[153] S. Singh, V.K. Rattan, S. Kapoor, R. Kumar and A. Rampal, J. Chem. Eng. Data **50**, 288–292 (2005). doi:10.1021/je049661s.
[154] F. London, Trans. Faraday Soc **33**, 8b–26 (1937). doi:10.1039/tf937330008b.
[155] O. Wallach, Justus. Liebigs. Ann. Chem. **414**, 233–243 (1918). doi:10.1002/jlac.v414:2.
[156] O. Wallach, Justus. Liebigs. Ann. Chem. **286**, 90–118 (1895). doi:10.1002/jlac.v286:1.
[157] N. Gel'perin and N. Zelenetskii, Russ. J. Phys. Chem. **34**, 1059–1061 (1960).
[158] G.G. Henderson, J.A.R. Henderson and I.M. Heilbron, Ber. Deutsch. Chem. Ges. **47**, 876–887 (1914). doi:10.1002/cber.v47:1.
[159] N. Zelinsky, Ber. Deutsch. Chem. Ges. **34**, 2877–2884 (1901). doi:10.1002/cber.v34:2.
[160] P. Sabatier and A. Mailhe, Synthesis **3**, 527–574 (1980).
[161] Y.S. Cheng, W.L. Liu and S.H. Chen, Synthesis **1980**, 223–224 (1980). doi:10.1055/s-1980-28975.
[162] J. Kenyon and R.H. Pickard, J. Chem. Soc., Trans. **107**, 35–62 (1915). doi:10.1039/CT9150700035.
[163] A.I. Vogel, J. Chem. Soc 1323–1338 (1938). doi:10.1039/jr9380001323.
[164] M. Frenkel, R.D. Chirico, V. Diky, X. Yan, Q. Dong and C. Muzny, J. Chem. Inf. Model. **45**, 816–838 (2005). doi:10.1021/ci050067b.
[165] R.E. Thek and L.I. Stiel, AIChE J. **12**, 599–602 (1966). doi:10.1002/aic.v12:3.
[166] E. Vanstone, J. Chem. Soc. Trans. **95**, 590–604 (1909). doi:10.1039/CT9099500590.